Controls on Timing of Hydrothermal Fluid Flow in South-Central Kansas, North-Central Oklahoma, and the Tri-State Mineral District

Sahar Mohammadi[1] (sahar@ku.edu), Andrew M. Hollenbach[1,2] (ahollenbach@ku.edu),
Robert H. Goldstein[2] (gold@ku.edu), Andreas Möller[2] (amoller@ku.edu), and Caroline M. Burberry[3] (cburberry2@unl.edu)

[1]*Kansas Geological Survey, University of Kansas, Lawrence, Kansas, USA*
[2]*KICC, Department of Geology, University of Kansas, Lawrence, Kansas, USA*
[3]*Department of Earth and Atmospheric Sciences, University of Nebraska-Lincoln, Lincoln, Nebraska, USA*

ABSTRACT

Paleozoic sedimentary rocks in the southern midcontinent of the United States have been affected by multiple events of deformation and fluid flow, resulting in petroleum migration, thermal alteration, Mississippi Valley-type mineralization, and a complex diagenetic history. This record is a hidden history of how cratonal settings respond to tectonic and non-tectonic drivers. The aim of this contribution is to better understand the controls on fluid migration in Paleozoic strata to evaluate whether hydrothermal activity is forced by tectonic or non-tectonic processes.

This paper summarizes and vets the distribution of published dates related to thermal events in the southern midcontinent. In addition, we present new U-Pb dates obtained by laser ablation–inductively coupled plasma–mass spectrometry (LA-ICP-MS) on calcite cements that were formed from hydrothermal fluids. These are from three samples from the Berexco Wellington KGS 1-32 core in Sumner County, Kansas; an ore sample from the Tri-State Mineral District, Neck City, Missouri; and a core sample from the Blackbird 4-33 well in Osage County, Oklahoma. Previous studies of these calcite samples provided evidence for hydrothermal fluid flow, with one of the Wellington samples possibly recording vertical hydrothermal fluid flow out of the basement.

The sample from the Tri-State Mineral District (Missouri) yields a mid-Cretaceous age of 115.6±3.1 Ma. This age falls into the timing of the Sevier Orogeny along the west coast and the development of its foreland basin in the midcontinent. Calcites from the Mississippian interval in the Wellington KGS 1-32 core yield dates of 305±10.5 Ma and 305.1±9.1 Ma. Calcite in Mississippian strata from the Blackbird 4-33 core yields a date of 308.6±2.5 Ma. These dates from Mississippian calcite cements indicate hydrothermal fluid flow in the Late Pennsylvanian that coincides with the timing of the Marathon-Ouachita Orogeny or the Ancestral Rocky Mountains Orogeny. A calcite sample from the Ordovician Arbuckle Group from the Berexco Wellington KGS 1-32 core yielded an age of 5.6±1.6 Ma,

coinciding with a time after high elevation uplift of the Rocky Mountains was already far advanced. We propose that this hydrothermal fluid flow may have been associated with increased meteoric recharge and increased regional fluid pressure in a basement aquifer that activated local seismic events far into the continental interior.

The distribution of ages of hydrothermal fluid flow confirms a syntectonic driver during the Ouachita Orogeny and Ancestral Rocky Mountains Orogeny deformation. Continuation of hydrothermal fluid flow well into the Permian and tailing off early in the Triassic indicates a post-tectonic driver, where uplifted areas continued to provide the recharge from gravity-driven fluid flow, until the mountains were mostly beveled by the early part of the Triassic. A dearth of Triassic and Jurassic hydrothermal events suggests Gulf of Mexico rifting and extension were less important. Rejuvenation of hydrothermal fluid flow in the Cretaceous and continuing into the Paleogene indicates that elevation and regional flexure from both the Sevier and Laramide events continued to drive hydrothermal fluid flow far from the main sites of mountainous uplift and deformation. Finally, hydrothermal fluid flow associated with more recent uplift of the Rocky Mountains may have been activated by recharge events that pressurized a regional basement aquifer and triggered seismic activity.

INTRODUCTION
AND GEOLOGICAL BACKGROUND

Abundant prior studies in the Tri-State Mineral District (Shelton et al., 1992; Gregg and Shelton, 2012; Ramaker et al., 2015; Bailey, 2018; Goldstein et al., 2019; Mohammadi et al., 2019a, 2019b; Temple et al., 2020) have suggested that tectonic drivers such as the Marathon-Ouachita/Ancestral Rocky Mountains or the Laramide orogenies may have led to hydrothermal fluid flow in the midcontinent. In south-central Kansas, for example, geochemical and fluid inclusion data yield paleotemperatures higher than normal burial temperatures from Ordovician-Pennsylvanian strata, indicating regional advective fluid migration from the basin to the foreland shelf (Walton et al., 1995; Goldstein et al., 2019). Late calcites with highly radiogenic $^{87}Sr/^{86}Sr$ also suggest fault (seismic) pumping from the basement, possibly during Laramide reactivation (King and Goldstein, 2018; Goldstein et al., 2019).

The Tri-State Mineral District (Missouri, Kansas, and Oklahoma) is one of the largest and best-studied Mississippi Valley-type (MVT) lead-zinc deposit regions in North America. Typical for MVT deposits, migration of warm brines deposited ore and gangue minerals (Leach et al., 2010). Ores in the district are mostly hosted in Mississippian rocks but are also known in lower Paleozoic and Pennsylvanian strata (Hagni, 1986; Shelton et al., 1992; Gregg and Shelton, 2012; Wenz et al., 2012). The widespread record of hydrothermal fluids and thermal alteration indicates a regionally advective system of fluid flow with stratigraphic and structural control (Goldstein et al., 2019). Many studies in the Tri-State Mineral District have focused on hydrothermal activity associated with lead-zinc ores as well

as calcite in caves (e.g., Fowler, 1933; Ridge, 1936; Schmidt, 1962; Noble, 1963; Kesler et al., 2004; Paradis et al., 2008; Gregg and Shelton, 2012; Wenz et al., 2012).

Published dates on minerals that precipitated from hydrothermal fluids strongly suggest multiple fluid flow events in the midcontinent, some triggered by tectonic drivers (table 1; fig. 1). As an example, in the Tri-State Mineral District, several periods of hydrothermal activity have been identified by U-Th-Pb dating of calcite. The first stage of hydrothermal mineralization with high salinity and high-temperature fluid inclusions occurred either at 251±11 Ma (Brannon et al., 1996) or earlier, in the Pennsylvanian, at ~290–320 Ma (Hagni and Grawe, 1964). Calcite cement with high salinity aqueous and oil inclusions at the Oronogo Circle deposit (Blasch and Coveney, 1988) yielded an age of 137±3 Ma. Calcite ages in the Picher Field mine (67±3 Ma) and Bendelari and Admiralty mines (39±2 Ma) suggest precipitation at the beginning and end of the Laramide Orogeny (Coveney et al., 2000). Nearby in northern Arkansas, U-Pb dating of coarse hydrothermal calcite in caves (Tennyson et al., 2017) yielded an age of 52±2 Ma, also coinciding with the Laramide Orogeny. Tennyson et al. (2017) suggested five tectonic events responsible for injecting advective fluids into the MVT districts in the Tri-State area and northern Arkansas.

The distribution of ages relevant to thermal history in the midcontinent (fig. 1) allows analysis of the degree to which hydrothermal fluid flow was caused by the Marathon-Ouachita/Ancestral Rocky Mountains Orogeny, Gulf of Mexico extension, the Sevier Orogeny, a thermal signature associated with isolated mid-Cretaceous intrusives, the Laramide Orogeny, the tectonic drivers

for the uplift of the Rocky Mountains and Colorado Plateau, or some other record of hydrothermal fluid flow that was not controlled by tectonics. Thus, our fundamental questions for this study are the following:

1. How does subsurface hydrothermal fluid flow in the midcontinent respond to the tectonic drivers at the continental margins?
2. What drivers have an impact on hydrothermal fluid flow?
3. What drives crustal deformation in the midcontinent?

To begin to answer these questions, this study compiles age data from the literature (fig. 1) and introduces new U-Pb age data from calcite samples that were known (from previous work) to have precipitated from hydrothermal fluids (fig. 2). The results show that U-Pb dating by laser ablation–inductively coupled plasma–mass spectrometry (LA-ICP-MS) can provide the age information needed to evaluate whether hydrothermal activity is correlated to various tectonic drivers or whether there is forcing that is not tectonic in origin. Three new dates show that there was hydrothermal fluid flow during the Pennsylvanian, related to either the Marathon-Ouachita Orogeny or Ancestral Rocky Mountains Orogeny. One new date supports an event of hydrothermal fluid flow concurrent with the Sevier Orogeny and the development of its foreland basin. Another new date reveals an event at or after ca. 5 Ma in a study area that is seismically active today, indicating that continued seismicity without a prominent orogenic driver can cause hydrothermal fluid flow. Finally, the distribution of new and published thermally relevant ages indicates that although some events of hydrothermal fluid flow were coincident with the Marathon-Ouachita/Ancestral Rocky Mountains deformation, many events continued well after that deformation had ceased.

The results show that the history of hydrothermal fluid flow is not simply a record of deformation, but one driven by a combination of tectonics, hydrogeology, and topography.
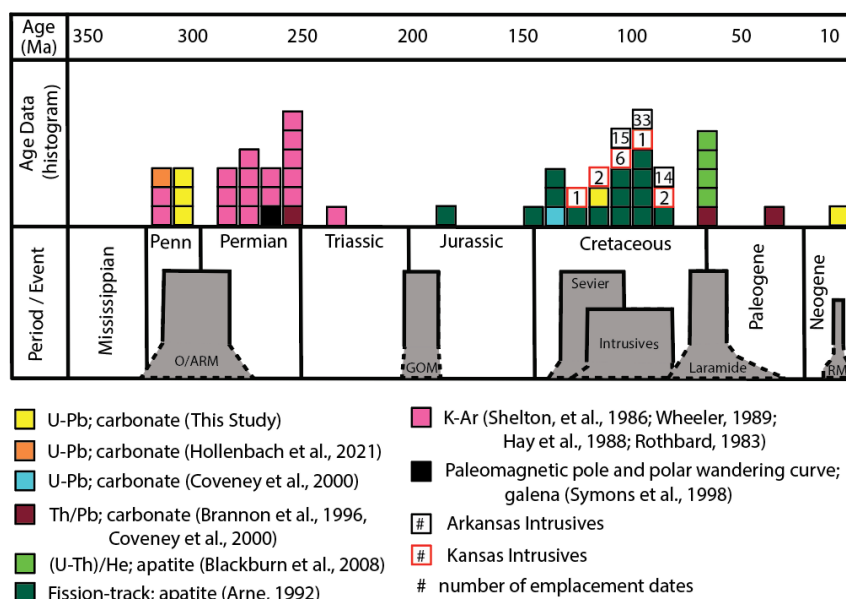
Figure 1. Summary of thermally relevant dates in the midcontinent, United States. Studies have been vetted to eliminate unreliable or irrelevant age data. Details in table 1. Ages can be compared to Marathon-Ouachita/Ancestral Rockies Orogeny (O/ARM), Gulf of Mexico rifting and extension (GOM), Sevier Orogeny, thermal signature associated with isolated Cretaceous intrusives, Laramide Orogeny, and tectonic drivers for uplift of the Rocky Mountains and Colorado Plateau (RM).

Figure 2. Basement fault map within the present study area, after Berendsen and Blair (1991), Northcutt and Campbell (1996), Dicken et al. (2001), and USGS (2020). Colored symbols show sample locations for this project.
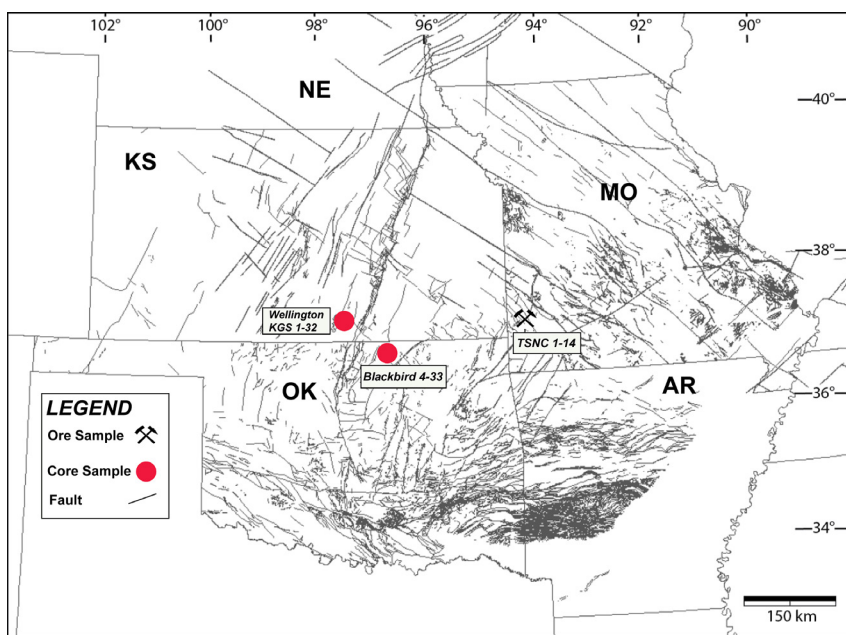
Table 1. Summary of thermally related dates in the midcontinent United States.

District	Locality	Date (Ma)	Dating Technique	Mineral	Geologic Period or Epoch	Tectonic Event	Reference
Tri-State MVT	Oronogo, MO	137±3	U-Pb	Calcite	Cretaceous	Laramide Orogeny	Coveney et al., 2000
	Picher, OK	67±3	Th-Pb	Calcite	Cretaceous boundary to Paleogene		
	Bendelari and Admiralty Mine	39±2	Th-Pb	Calcite	Eocene		
East Kansas	Jumbo Mine	251±11	Th-Pb	Calcite	Late Permian–Early Triassic	Late Paleozoic Alleghenian–Ouachita Orogeny	Brannon et al., 1996
Central Arkansas	Little Rock, AR; Mississippian (Jackfork Fm.)	117.1±20.9	Apatite fission track	Apatite	Cretaceous	Uplift and erosion	Arne, 1992
	Hollis, AR; Mississippian (Jackfork Fm.)	102.5±27.1	Apatite fission track	Apatite	Cretaceous		
	Lake Hamilton, AR; Mississippian (Stanley Shale)	130.2±6.3	Apatite fission track	Apatite	Cretaceous		
	Ferndale, AR; Ordovician (Womble Shale)	95.2±10.7	Apatite fission track	Apatite	Cretaceous		
	North Little Rock, AR; quartz vein	98.6±17.7	Apatite fission track	Apatite	Cretaceous		
	Conway, AR; Pennsylvanian (Atoka Fm.)	140.9±8.4	Apatite fission track	Apatite	Cretaceous		
Arkoma Basin	Plumerville, AR; Pennsylvanian (Atoka Fm.)	130.3±8.7	Apatite fission track	Apatite	Cretaceous		
	Atkins, AR; Pennsylvanian (Atoka Fm.)	128.2±5.8	Apatite fission track	Apatite	Cretaceous		
	Ludwig, AR; Pennsylvanian (Atoka Fm.)	183.6±11.7	Apatite fission track	Apatite	Jurassic		
	Ozark, AR; Pennsylvanian (Atoka Fm.)	98.2±23.1	Apatite fission track	Apatite	Cretaceous		

Ouachita Fold Belt	Lake Ouachita, AR; Lower Ordovician (Womble Shale)	262±10	K-Ar	Adularia	Permian		Shelton et al., 1986
Arbuckle Mountain, Oklahoma	Arbuckle Mountains, OK	286±23	K-Ar	K-Feldspar	Late Pennsylvanian-Early Permian	Ancestral Rocky Mountains Uplift	Wheeler, 1989
		285±23	K-Ar	K-Feldspar	Late Pennsylvanian-Early Permian		
		283±23	K-Ar	K-Feldspar	Late Pennsylvanian-Early Permian		
		235±23	K-Ar	K-Feldspar	Permian		
		266±26	K-Ar	K-Feldspar	Permian		
East Missouri	Along Mississippi River; (Upper Ordovician "Deicke" tuff)	390.1±6.3	K-Ar	K-Feldspar	Devonian	Major episode of midcontinent epeirogeny, Ouachita Orogeny	Hay et al., 1988
		367.9±2.0	Rb-Sr	K-Feldspar	Devonian		
		272.5±5.5	K-Ar	Illite; smectite	Permian		
		271.5±4.3	K-Ar	Illite; smectite	Permian		
		258.9±4.1	K-Ar	Illite; smectite	Permian		
		265.6±4.2	K-Ar	Illite; smectite	Permian		
		257.6±4.1	K-Ar	Illite; smectite	Permian		
		257.7±4.1	K-Ar	Illite; smectite	Permian		
		279.3±4.5	K-Ar	Illite; smectite	Permian		
		315.9±4.9	K-Ar	Illite; smectite	Pennsylvanian		
		317.9±6.2	K-Ar	Illite; smectite	Pennsylvanian		
		254.4±4.0	K-Ar	Illite; smectite	Permian		
Southeast Missouri	Ozark Dome	312 to 262 (Kiaman Superchron)	Paleo-magnetic pole and polar wander	Magnetite spheroids	Pennsylvanian–Early Permian or later	Late-Paleozoic Alleghenian–Ouachita Orogeny	Wisniowiecki et al., 1983; Leach et al., 2001
	Along west side St. Francois Mtn.; Bonneterre Dolomite	273±10	Paleo-magnetic pole and polar wander	Galena	Early Permian	Late-Paleozoic Alleghenian-Ouachita Orogeny	Symons et al., 1998
	Viburnum Trend; Lamotte Sandstone	255±15	K-Ar	Illite	Permian	Late Paleozoic Ouachita Orogeny	Rothbard, 1983
Central Missouri		312 to 262 (Kiaman Superchron)	Paleo-magnetic pole and polar wander	Magnetite in barite galena and sphalerite	Late Pennsylvanian to Early Permian	Alleghenian Orogeny	Symons and Sangster, 1991

North Arkansas		265±20	Paleo-magnetic pole and polar wander		Permian	Alleghenian-Ouachita Orogeny	Pan and Symons, 1990; Leach et al., 2001
		52±2	U-Pb		Eocene	Laramide Orogeny	Tennyson et al., 2017
Northeast Kansas	Leonardville Kimberlite	66.1±8	(U-Th)/(He)	Apatite	Late Cretaceous to Paleogene	Laramide reactivation	Blackburn et al., 2008
	Bala Kimberlite	64.3±7.5	(U-Th)/(He)	Apatite	Late Cretaceous to Paleogene	Laramide reactivation	
	Stockdale Kimberlite	67.3±4.4	(U-Th)/(He)	Apatite	Late Cretaceous to Paleogene	Laramide reactivation	
	Tuttle Kimberlite	67.2±5.1	(U-Th)/(He)	Apatite	Late Cretaceous to Paleogene	Laramide reactivation	
Kansas Intrusives	Bala Kimberlite	103.0±7.5	(U-Th)/(He)	Magnetite	Cretaceous	Intrusive	Blackburn et al., 2008
	Stockdale Kimberlite	102.9±11	(U-Th)/(He)	Titanite (non-abraded)	Cretaceous	Intrusive	
	Stockdale Kimberlite	106.9±3.1	(U-Th)/(He)	Titanite (abraded)	Cretaceous	Intrusive	
	Baldwin Creek Kimberlite	85.5±2.3	(U-Th)/(He)	Apatite	Cretaceous	Intrusive	
	Baldwin Creek Kimberlite	88.4±2.7	Rb-Sr	Phlogopite	Cretaceous	Intrusive	
	Tuttle Kimberlite	108.6±9.6	(U-Th)/(He)	Zircon (10 grains)	Cretaceous	Intrusive	
	Tuttle Kimberlite	103.9±14.1	(U-Th)/(He)	Titanite (14 grains)	Cretaceous	Intrusive	
	Tuttle Kimberlite	98.8±8.9	(U-Th-[Sm])/(He)	Megacrystic garnet (9 aliquots)	Cretaceous	Intrusive	
	Tuttle Kimberlite	106.6±1.0	Rb-Sr	Phlogopite (5); clinopyroxene (1)	Cretaceous	Intrusive	
	Stockdale Kimberlite	123±12	Fission track	Apatite from granite xenolith	Cretaceous	Intrusive	Brookins & Naeser, 1971
	Bala Kimberlite	115±12	Fission track	Apatite from granite xenolith	Cretaceous	Intrusive	
	Stockdale Kimberlite	112±6	K-Ar	Chloritized biotite from granite xenolith in kimberlite	Cretaceous	Intrusive	

Central Arkansas Intrusives	Prairie Creek	99±2	K-Ar	Phlogopite; lamproite	Cretaceous	Intrusive	Zartman, 1977
		108±3	K-Ar	Phlogopite; lamproite	Cretaceous	Intrusive	
		106±3	K-Ar	Phlogopite; lamproite	Cretaceous	Intrusive	Gogineni et al., 1978
	Magnet Cove	97±5	K-Ar	Biotite; melteigite; ijolite	Cretaceous	Intrusive	Zartman et al., 1967
		100±5	K-Ar	Biotite; melteigite; ijolite	Cretaceous	Intrusive	
		102±8	Rb-Sr	Biotite; ijolite	Cretaceous	Intrusive	
	Granite Mtn.	89±4	K-Ar	Biotite; nepheline syenite	Cretaceous	Intrusive	
		94±5	K-Ar	Biotite; nepheline syenite	Cretaceous	Intrusive	
		89±3	Rb-Sr	Biotite; nepheline syenite	Cretaceous	Intrusive	
		87.9±6.4	Fission track	Apatite	Cretaceous	Intrusive	Arne, 1992
	Magnet Cove	103.8±4.3	Fission track	Apatite	Cretaceous	Intrusive	
		100.3±6.5	Fission track	Apatite	Cretaceous	Intrusive	
		97.4±6.8	Fission track	Apatite	Cretaceous	Intrusive	
		94.4±0.2	40Ar/39Ar	Biotite; ijolite; jacupirangite	Cretaceous	Intrusive	Baksi, 1997
		94.2±0.2	40Ar/39Ar	Biotite; ijolite; jacupirangite	Cretaceous	Intrusive	
		89.6±0.5	40Ar/39Ar	Biotite; ijolite; jacupirangite	Cretaceous	Intrusive	
		90±9	Fission track	Apatite; carbonatite	Cretaceous	Intrusive	Scharon and Hsu, 1969
		103±10	Fission track	Apatite; carbonatite	Cretaceous	Intrusive	
		105±10	Fission track	Apatite; titanite; syenite	Cretaceous	Intrusive	
		102±4	K-Ar	Whole rock; trachyte	Cretaceous	Intrusive	Baldwin and Adams, 1971
	Potash Sulfur Springs	100±2	U-Pb	Zircon; feldspathoidal syenite	Cretaceous	Intrusive	Zartman and Howard, 1987

Dare Mine Knob	106.3±1.1	40Ar/39Ar	Whole rock; lamproite	Cretaceous	Intrusive	Eby and Vasconcelos, 2009
	106.6±1.1	40Ar/39Ar	Whole rock; lamproite	Cretaceous	Intrusive	
V-intrusive	102.3±10.1	Fission track	Apatite; microijolite	Cretaceous	Intrusive	
	98.7±17.9	Fission track	Titanite; syenite	Cretaceous	Intrusive	
	98.3±6.5	Fission track	Apatite; malignite	Cretaceous	Intrusive	
	96.4±17	Fission track	Titanite; malignite	Cretaceous	Intrusive	
Potash Sulphur Springs	102.7±9.3	Fission track	Apatite; carbonatite	Cretaceous	Intrusive	
	100.8±8.0	Fission track	Apatite; ijolite	Cretaceous	Intrusive	
	99.4±8.4	Fission track	Apatite; ijolite	Cretaceous	Intrusive	
Magnet Cove	94.5±1.3	40Ar/39Ar	Mica; phlogopite; carbonatite	Cretaceous	Intrusive	
	94.0±1.2	40Ar/39Ar	Mica; phlogopite; carbonatite	Cretaceous	Intrusive	
	98.7±17.8	Fission track	Apatite; phonolite	Cretaceous	Intrusive	
	98.4±9.8	Fission track	Titanite; phonolite	Cretaceous	Intrusive	
	96.3±8.7	Fission track	Apatite; jacupirangite	Cretaceous	Intrusive	
	97.3±9.7	Fission track	Titanite; jacupirangite	Cretaceous	Intrusive	
	95.7±6.4	Fission track	Apatite; carbonatite	Cretaceous	Intrusive	
	96.9±22.3	Fission track	Titanite; syenite	Cretaceous	Intrusive	
	95.8±5.7	Fission track	Apatite; syenite	Cretaceous	Intrusive	
	95.1±11.7	Fission track	Apatite; ijolite	Cretaceous	Intrusive	
	97.7±36.2	Fission track	Titanite; ijolite	Cretaceous	Intrusive	
	95.9±14.4	Fission track	Apatite; syenite	Cretaceous	Intrusive	
	96.7±7.8	Fission track	Apatite; ijolite	Cretaceous	Intrusive	
	96.0±8.4	Fission track	Apatite; ijolite	Cretaceous	Intrusive	
	96.3±17.6	Fission track	Apatite; carbonatite	Cretaceous	Intrusive	
	98.5±8.4	Fission track	Apatite; ijolite	Cretaceous	Intrusive	
	98.4±9.9	Fission track	Titanite; phonolite	Cretaceous	Intrusive	

	Benton dikes	98.1±9.7	Fission track	Apatite; camptonite	Cretaceous	Intrusive	
		97.3±23.5	Fission track	Titanite; sannaite	Cretaceous	Intrusive	
	Morrilton-Perryville carbonatites	98.9±6.7	Fission track	Apatite; breccia	Cretaceous	Intrusive	
	Morrilton-Perryville carbonatites	99.0±9.2	Fission track	Apatite; carbonatite	Cretaceous	Intrusive	
	Saline County	86.8±25.1	Fission track	Apatite; syenite	Cretaceous	Intrusive	
		89.9±8.6	Fission track	Titanite; syenite	Cretaceous	Intrusive	
	Granite Mountain	89.7±16.7	Fission track	Apatite; syenite	Cretaceous	Intrusive	
		87.1±12.4	Fission track	Titanite; syenite	Cretaceous	Intrusive	
		90±11.2	Fission track	Apatite; syenite	Cretaceous	Intrusive	
		88.1±9.1	Fission track	Apatite; syenite	Cretaceous	Intrusive	
		88.1±13	Fission track	Titanite; syenite	Cretaceous	Intrusive	
		89.7±9.4	Fission track	Apatite; syenite	Cretaceous	Intrusive	
		85.8±11.7	Fission track	Apatite; syenite	Cretaceous	Intrusive	
		86.1±13.3	Fission track	Titanite; syenite	Cretaceous	Intrusive	
		88.7±9.9	Fission track	Titanite; pegmatite	Cretaceous	Intrusive	
North-Central Oklahoma	Major County, OK	318±20	U-Pb	Calcite	Early Pennsylvanian	Alleghenian-Ouachita Orogeny	Hollenbach et al., 2021
North-Central Oklahoma	Osage County, OK	308.6±2.5	U-Pb	Calcite	Late Pennsylvanian	Marathon-Ouachita Orogeny	This study
Tri-State MVT	Neck City, MO	115.6±3.1	U-Pb	Calcite	Early Cretaceous	Sevier Orogeny	
South-Central Kansas	Sumner County, KS	5.6±1.6	U-Pb	Calcite	Neogene		
		305±10.5	U-Pb	Calcite	Late Pennsylvanian	Marathon-Ouachita Orogeny	
		305.1±9.1	U-Pb	Calcite	Late Pennsylvanian	Marathon-Ouachita Orogeny	

METHODS AND RESULTS

The authors conducted a literature review to compile and vet all previously published dates that were related to hydrothermal processes in the midcontinent (table 1). The vetting process involved excluding previously published dates if the date was older than the depositional age, if the mineral was known to be altered, if the mineral did not result from a thermal process, or if dating of a sample was superseded by a more reliable method (e.g., K-Ar dates that are prone to be compromised by K mobility).

Five samples from the Nemaha Uplift and Tri-State Mineral District were prepared for U-Pb dating of calcite cement. The calcite partially filled breccia and vugular pores. All samples were chosen because previous peer-reviewed work had demonstrated a hydrothermal origin (see table 2) and because of the diverse hypotheses that had been published about their timing (King, 2013; King and Goldstein, 2018; Goldstein et al., 2019; Mohammadi et al., 2019b). One sample is from the Tri-State Mineral District (an ore sample — TSNC 1-14) from Neck City, Missouri. Another comes from near the base of the Berexco Wellington KGS 1-32 core (Sumner County, Kansas), at a depth of 5,061.5 ft (~1.54 km) in the Arbuckle Group. Two more come from the Berexco Wellington KGS 1-32 core's Mississippian stratigraphic interval at depths of 3,775.5 and 3,758.9 ft (~1.15 km). Another sample is from a depth of 3,370.9 ft (~1.03 km) (Mississippian strata) from the Blackbird 4-33 core in Osage County, Oklahoma (fig. 2). This study used LA-ICP-MS to obtain absolute radiometric ages for calcite cement within established (petrography, fluid inclusion, isotope geochemistry, cathodoluminescence [CL] imaging)

paragenetic frameworks. U-Pb analyses for this project were conducted on 100 μm-thick polished sections at the Department of Geology, University of Kansas, with a Thermo Scientific Element2 ICP-MS attached to a Photon Machines Analyte.G2 193 nm ArF excimer laser. Circular spots of 130 μm diameter were ablated with 2.5 J cm^{-2} laser fluence at 10 Hz repetition rate for 30 seconds, resulting in 20 μm deep pits. Helium was the carrier gas, tied in with argon gas before entry into the ICP-MS. Laser-induced fractionation, including isotope and elemental fractionation, and calibration drift were corrected by bracketing unknowns with NIST614 glass reference material of known Pb isotope ratio (Woodhead and Hergt, 2001) and the calcite reference material WC-1 (Roberts et al., 2017) for U-Pb fractionation. Calcite reference material DBTL (Hill et al., 2016) was used for validation of the results to ensure that the U-Pb calibration yielded correct dates. Data reduction used the IOLITE software package (Paton et al., 2010, 2011) for calibration of the Pb-isotope ratio and a second step for U-Pb fractionation correction.

The new radiometric results for the sample from the Tri-State Mineral District (TSNC 1-14) give a mid-Cretaceous lower intercept at 115.6±3.1 Ma. The sample from the Wellington KGS 1-32 core in the Arbuckle Group (depth of 5,061.5 ft [~1.54 km]) has Pb near the detection limit; the resulting age is 5.6±1.6 Ma (fig. 3a–b). Samples from the Wellington KGS 1-32 core in Mississippian strata (depth of 3,775.5 and 3,758.9 ft [~1.15 km]) result in ages of 305±10.5 Ma and 305.1±9.1Ma (fig. 3c–d). The sample from the Blackbird 4-33 core, also in Mississippian strata (depth of 3,370.9 ft [~1.03 km]), produced an age of 308.6±2.5 Ma (fig. 3E). Supplementary data are listed in table S1.

Table 2. Summary of data from homogenization temperature (T_h), T_m ice (wt. % NaCl eq.), strontium isotope, and oxygen isotope (‰) from previously published studies (King and Goldstein, 2018; Goldstein et al., 2019; Mohammadi et al., 2019b) evidence for hydrothermal processes.

| Sample ID	Location	Geologic System (depth in feet)	T_h (°C) P-primary; S-secondary	Calculated Salinity (wt. % eq. NaCl)	δ18O‰ (VPDB)	$^{87}Sr/^{86}Sr$
TSNC 1-14	Neck City, MO	Mississippian	P-60 to 98	5.4 to 8.5	-11.04	0.7099
Blackbird 4-33 core	Osage Co., OK	Mississippian (3,370.9)	P-86.2 to 173	3 to 24.3	-6.21	0.7112
Berexco Wellington KGS 1-32 core	Sumner County, KS	Ordovician (Arbuckle Group; 5,061.5)	S-70.5 to 89.8	18.2 to 19.6	-8.6 to -9.5	0.71572
Berexco Wellington KGS 1-32 core	Sumner County, KS	Mississippian (3,775.5)	P-91.0 to 103.5; S-67.0 to 83.0	P-14.5 to 15.5; S-19.6 to 19.9	-8.4 to -9.5	0.70845
Berexco Wellington KGS 1-32 core	Sumner County, KS	Mississippian (3,758.9)			-8.5 to -9.0	0.70842
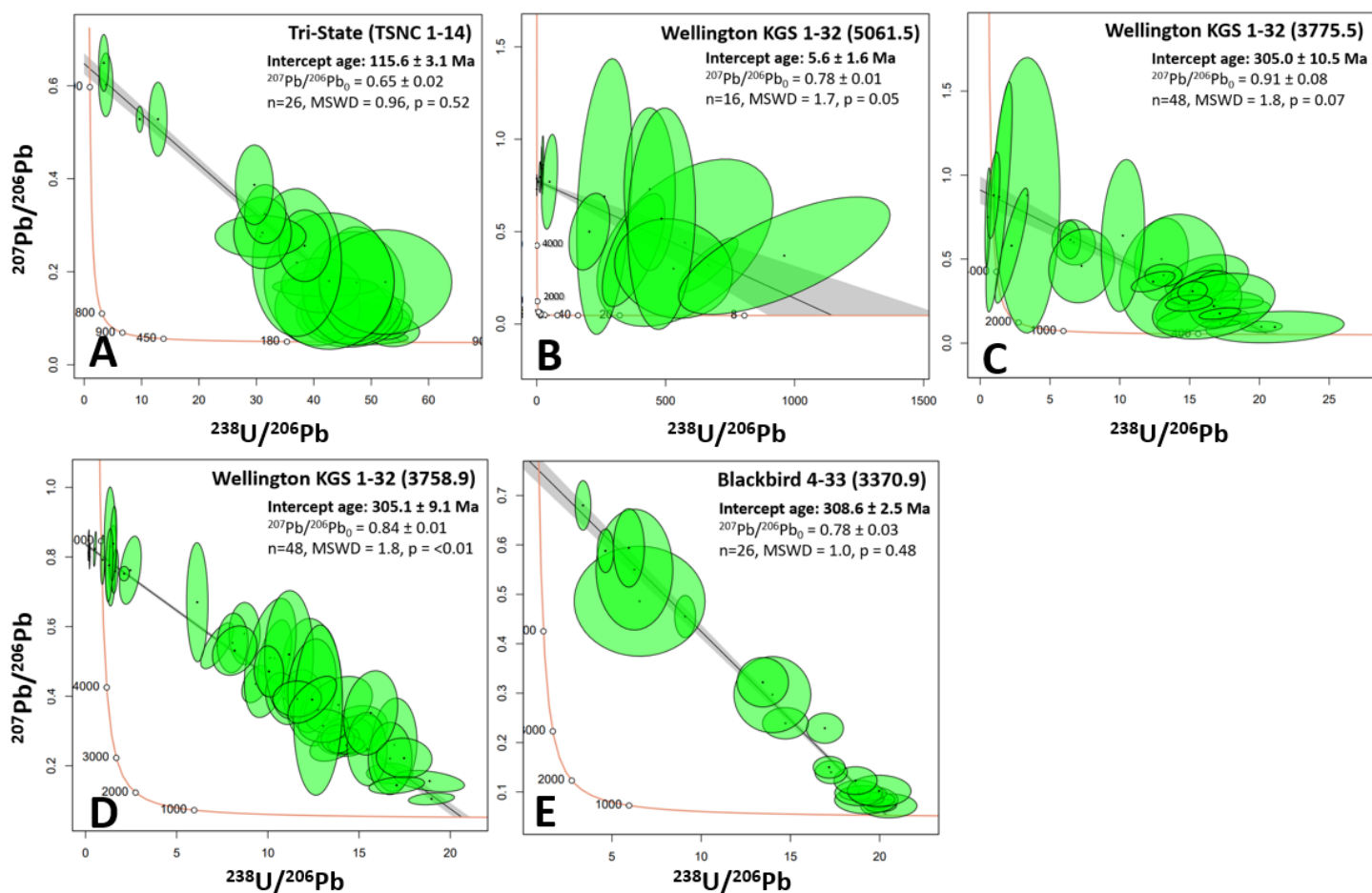
Figure 3. Tera-Wasserburg Concordia diagrams for U-Pb data from calcite with fluid inclusion, petrographic, and geochemical evidence for hydrothermal processes (see table 2). Samples from (A) Missouri (TSNC 1-14) — Cretaceous age (115.6±3.1 Ma) consistent with a Sevier Orogeny driver outside of the age envelope for Laramide or intrusive activity nearby; (B) Kansas (Wellington, 5,061.5 ft) — Late Miocene to Pliocene age (5.6±1.6 Ma) for hydrothermal fluid flow in breccia-filling calcite, indicating continued seismicity unrelated to a known tectonic driver; (C and D) Kansas (Wellington, 3,775.5 ft, and Wellington, 3,758.9 ft) — Late Pennsylvanian age (305±10.5 and 305.1±9.1 Ma), consistent with the Marathon-Ouachita Orogeny or Ancestral Rocky Mountains Orogeny; and (E) Oklahoma (Blackbird 4-33, 3,370.9 ft)—Late Pennsylvanian age (308.6±2.5 Ma), consistent with the Marathon-Ouachita Orogeny or Ancestral Rocky Mountains Orogeny.

DISCUSSION

Implications of the 305±10.5 Ma and 305.1±9.1 Ma Ages for Calcite Cement in the Berexco Wellington KGS 1-32 Core and the 308.6±2.5 Ma Age for Calcite Cement in the Blackbird 4-33 Core

The two calcite samples from the Mississippian interval of the Berexco Wellington KGS 1-32 core (depths 3,775.5 and 3,758.9 ft) have been described by King (2013) and Goldstein et al. (2019). Primary and secondary fluid inclusion assemblages yielded consistent homogenization temperature (T_h) values in sample 3,775.5. Values in the four primary fluid inclusion assemblages (FIAs) ranged from 91.0 to 103.5 °C; the three secondary FIAs ranged from 67.0 to 83.0 °C. Melting temperature (T_m) ice measurements in the primary inclusions yielded salinities of 14.5–15.5 wt. % NaCl eq., and secondary fluid inclusions yielded T_m ice measurements of 19.6–19.9 wt. % NaCl eq. No fluid inclusion data were produced for sample 3,758.9. The two analyzed samples, however, essentially have the same δ18O (-8.4 to -9.5‰ for 3,775.5; -8.5 to -9.0‰ for 3,758.9) and $^{87}Sr/^{86}Sr$ (0.70845 for 3,775.5 and 0.70842 for 3,758.9) and thus likely have a common origin (table 2). The fluid inclusion data argue for an origin from a hydrothermal fluid, which Goldstein et al. (2019) ascribed to either regional advective fluid flow associated with uplift of the Ouachita Mountains and Ancestral Rocky Mountains or a late stage of fracture-controlled flow.

In a previous study by Mohammadi et al. (2019b) on breccia partially filling calcite cement in the Blackbird 4-33 core sample (Mississippian strata, Oklahoma), data from primary fluid inclusions showed T_h values of 86.2 to 173 °C and salinities of 3 to 24.3 wt. % NaCl eq. The wide range of T_h and salinity was interpreted to result from fluid mixing (Mohammadi et al., 2019b). δ18O value for the calcite is -6.21‰ VPDB and $^{87}Sr/^{86}Sr$ is 0.7112 (table 2).

Our new data from U-Pb analysis for these three samples give Late Pennsylvanian ages of 305±10.5, 305.1±9.1, and 308.6±2.5 Ma. These ages coincide with the timing of deformation and uplift associated with the Marathon-Ouachita Orogeny or Ancestral Rocky Mountains Orogeny (Flawn, 1961; Frezon and Dixon, 1975; Kluth and Coney, 1981; Ye et al., 1996; Marshak et al., 2003). These data support the idea that there is a tectonic driver for hydrothermal fluid flow and that at least some events of hydrothermal fluid flow correlate to events of deformation and uplift.

Implications of the 115.6±3.1 Ma Age for the Tri-State Calcite Cement

Mohammadi et al. (2019b) previously published fluid inclusion and isotope geochemistry data for the calcite sample from the Tri-State mine (TSNC 1-14), Neck City, Missouri. The sample came from a breccia pore in Mississippian strata. It yielded primary fluid inclusions with T_h values ranging from 60 to 98 °C, T_m ice salinities of 5.4 to 8.5 wt. % NaCl eq., and $^{87}Sr/^{86}Sr$ of 0.7099. Oxygen isotope value for this sample was -11.04 (per mil VPDB) (table 2). These data indicate the calcite precipitated from hydrothermal fluids moving through the karst breccias.

Previously, we suggested that migration of these hot and moderately saline fluids was most likely associated with the Ouachita Orogeny. However, our new data from U-Pb analysis for this specific sample gives the mid-Cretaceous age of 115.6±3.1 Ma. This age clearly coincides with the Sevier Orogeny along the western continental margin and development of its foreland basin well into the midcontinent. The age is too old to be ascribed to the Laramide Orogeny and inconsistent with ages of various intrusive rocks in the area.

The Sevier Orogeny is a diachronous event that deformed the western margin of North America during the Jurassic (southern reaches) to Eocene (northern reaches) and is characterized by thin-skinned deformation (Heller et al., 1986; Taylor et al., 2000; DeCelles, 2004; Yonkee and Weil, 2015). Most of that deformation was far afield from the study area, but the study region falls within the large foreland basin of the orogen, which was strongly downflexed and infilled by the Western Interior Seaway during the Cretaceous (DeCelles, 2004; Blakey and Ranney, 2018) as a result of loading from the thrust sheets to the west. The distant mountains and downflexing of the foreland basin (Wells et al., 2012) left hydrothermal fluid flow signatures in the calcite record of the midcontinent, showing that the midcontinent's record of hydrothermal fluid flow can respond to tectonic drivers at the continental margins in distant areas of flexure.

Implications of the 5.6±1.6 Ma Age for Calcite Cement in Berexco Wellington KGS 1-32

Calcite cements from the Berexco Wellington KGS 1-32 core in the Arbuckle Group (depth of 5,061.5 ft) have been identified in previous studies (King and Goldstein, 2018; Goldstein et al., 2019) as one of the latest events in the paragenesis and closely associated with the timing of sphalerite and galena precipitation. Cements toward the base of the Arbuckle Group occur in breccia and vug pores and have highly radiogenic $^{87}Sr/^{86}Sr$ around 0.716. These cements typically lack primary fluid inclusions but are crosscut by secondary fluid inclusions yielding T_h of 70.5

to 89.8 ℃ and T_m ice yielding salinities of 18.2 to 19.6 wt. % NaCl eq. δ18O values for the calcite range from -8.6‰ to -9.5‰ VPDB (table 2).

The conclusions from previous publications on this material were based on oxygen and strontium isotopic compositions; paragenetic, regional, and stratigraphic distribution of the calcite; and samples with primary fluid inclusions. Previous publications suggested that these late calcites resulted from a late stage of basement-involved fault pumping of hydrothermal fluids, where fluids were flowing vertically out of the basement into the overlying section during faulting events (King and Goldstein, 2018; Goldstein et al., 2019). Those fluids achieved high temperatures because they were sourced from deep in the basement. The source in the Proterozoic basement also explains the high strontium isotope ratio. The most feasible explanation for such flow is fault (seismic) pumping, where active motion reactivating deep-seated faults caused short-term injection of warm fluids from depth (Sibson et al., 1975). The paragenesis from the previous studies indicated that this deformation must have been after the Permian, and the studies hypothesized that far-field stresses from the Laramide Orogeny caused the fluid flow. However, our new 5.6±1.6 Ma age on the calcite indicates that the hydrothermal fluid flow was not during the Laramide Orogeny but occurred in the late Miocene to Pliocene. This young age for active fault pumping of hydrothermal fluids provides evidence for fluid drivers other than major continent-margin tectonic events. This 5.6±1.6 Ma fluid flow was followed by a later hydrothermal fluid, resulting in high-temperature secondary fluid inclusions.

To explain hydrothermal fluid flow at 5.6 Ma and later, we can consider that the Miocene-Pliocene fault pumping was caused by far-field stresses associated with the deformation that caused the broad regional uplift of the Rocky Mountains and Colorado Plateau (Eaton, 2008). If correct, the timing of uplift of the Rocky Mountains and Colorado Plateau should coincide with the 5.6±1.6 Ma date. Extensive literature addresses the uplift of the Rocky Mountains and Colorado Plateau, with work indicating that uplift is mostly caused by Neogene mantle convection and buoyancy related to low-density crust and upper mantle in the area (e.g., Karlstrom et al., 2012). Well-accepted paleo-elevation proxies indicate that the region had achieved half of its current elevation by the end of the Laramide Orogeny and reached its current elevation by about 16 Ma (Heitmann et al., 2021). A technique using vesicularity of basalts suggested slow uplift between 25 Ma and 5 Ma and rapid uplift after 5 Ma (Sahagian et al., 2002).

Apatite fission-track dating, track-length measurements, and apatite helium dating determined the timing of incision of various segments of the Grand Canyon. One segment formed at 70–50 Ma, another at 25–15 Ma, and two others formed in the past 5–6 million years, associated with integration of the Colorado River drainage (Karlstrom et al., 2012). Other regional data suggest acceleration of uplift after about 10 Ma (Aslan et al., 2010). Taken together, most of this work indicates that deformation and uplift began, accelerated, and was well advanced long before the 5.6±1.6 Ma calcite. Although some deformation continued after 5.6 Ma in the Rockies and Colorado Plateau (Eaton, 2008) and tilting of the High Plains continued (McMillan et al., 2002; Duller et al., 2012), our date does not coincide with the timing of the bulk of the uplift and deformation. Thus, the fault pumping that caused precipitation of the calcite is not easily explained simply by the far-field stresses associated with uplift of the Rocky Mountains and Colorado Plateau. Another driver must be proposed to explain fault-pumped hydrothermal fluid flow at 5.6±1.6 Ma and younger.

Here, we propose a hypothesis that could offer a reasonable explanation, a model that combines the already uplifted high elevation of the Rockies and High Plains with climate change that allowed groundwater recharge at high elevation. This recharge and high elevation induced hydraulic head that increased fluid pressure far into the continental interior (fig. 4). That fluid pressure triggered the fault movement. This idea is strongly supported by the modern-day regional aquifer configuration, where the Western Interior Plains Aquifer System (WIPAS), consisting of Cambrian-Mississippian strata, is recharged from the highlands to the west and shows regional eastward flow (Jorgenson et al., 1993; Musgrove and Banner, 1993). For the modern regional hydrogeology, the basement is normally considered to be the lower confining unit for the WIPAS, but if the basement rocks have the permeability to function as an aquifer, then high elevation of the Rocky Mountains and High Plains, with sufficient recharge, could have led to fluid charging and eastward flow through a basement aquifer. Townend and Zoback (2000) argued that basement rocks can maintain permeability, critically stressed faults, and hydrostatic pressures. Recent work on induced seismicity demonstrates that fluid pressure perturbations can trigger critically stressed faults in the basement (e.g., Ellsworth, 2013; Schoenball et al., 2018). Ancient fluid pressure changes could have triggered earthquakes that led to seismic pumping of hot fluids. The question is, when did the climate allow for sufficient
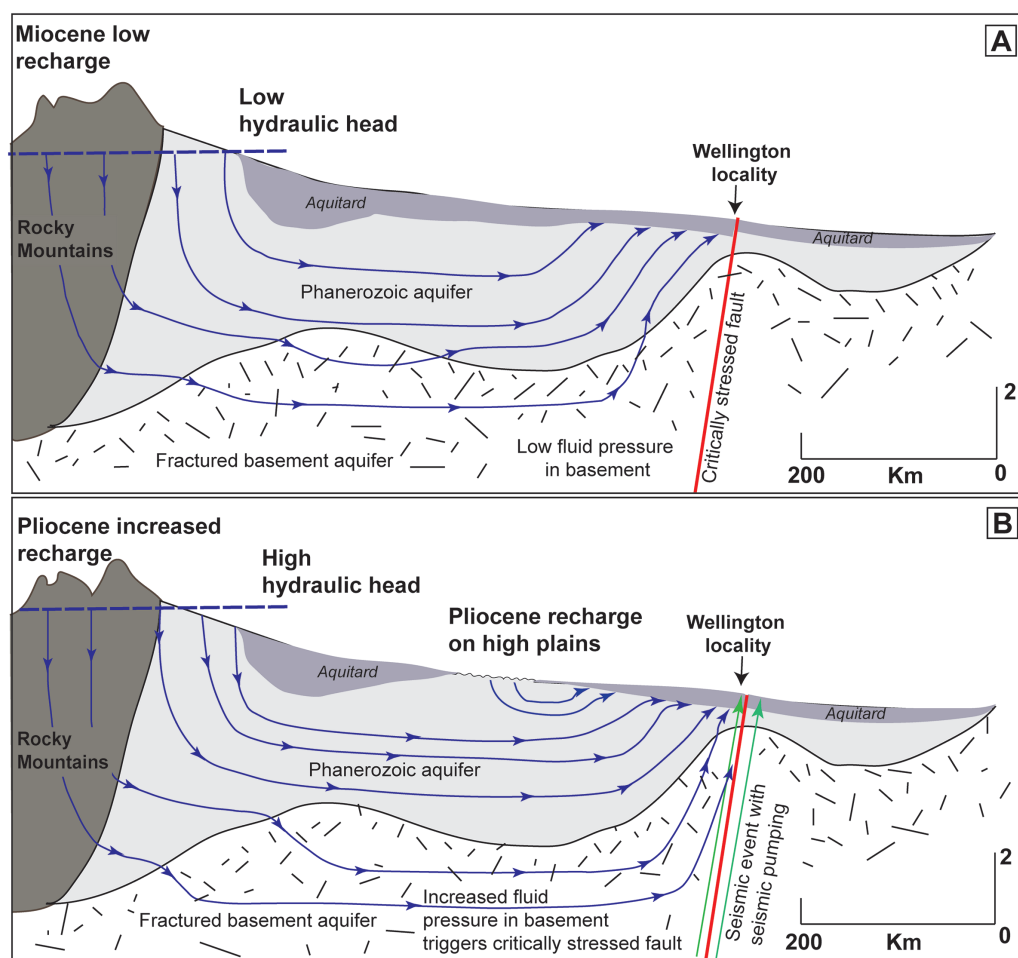
Figure 4. Conceptual model east-west cross section showing hypothesis for climate-change-induced hydrothermal fluid flow. Regional recharge in highlands allows eastward fluid flow in the Western Interior Plains Aquifer (WIPAS) and in the basement (modified from Garven and Raffensperger, 1997). (A) During relatively arid times in the Miocene, basement fluid pressure is relatively low and critically stressed faults to the east are not triggered. (B) During times of greater recharge in the Pliocene, water tables rise, increasing fluid pressure in critically stressed faults. Seismic events pump hot fluids from deep areas into more shallow zones.

recharge in the Rocky Mountains, Colorado Plateau, and western Great Plains to increase fluid pressure and trigger critically stressed faults?

Paleoclimate reconstructions of the Rocky Mountains, Colorado Plateau, and western Great Plains all show evidence of increasing rainfall after the late Miocene (Chapin, 2008). Middle to Late Miocene rocks show a record of relatively arid climate conditions. Beginning about 6 Ma, the transition to the Pliocene shows evidence for increased seasonal rainfall, leading to integration of drainages, incision of uplifts, and erosional incision of the Ogallala Formation. Strata of the Meade basin record this transition in southwest Kansas, with the Meade basin first created by erosional removal of evaporites and later filled with Pliocene (~4.5–3.2 Ma) sediments. Those Pliocene strata show evidence for locally waterlogged and subhumid conditions (Lukens et al., 2019). Similarly, Duller et al. (2012) concluded that there was a climate-induced increase in river discharge across the Miocene-Pliocene boundary for areas of western Nebraska. It has been proposed that this climate transition coincided with the development of seasonal rainfall associated with the beginning of the North American monsoon, caused by

and coincident with the opening of the Gulf of California (Chapin, 2008). After uplift was well underway, climate change to more humid conditions with more active recharge in the highlands led to increased hydraulic head and, therefore, increased fluid pressure (fig. 4). The recharge induced or stimulated eastward flow through the WIPAS and through the basement rocks. Where the increased fluid pressure encountered critically stressed faults in the basement, it triggered seismic events that led to fault pumping of hydrothermal fluids out of the basement and into the Arbuckle Group.

Implications of the Distribution of Ages for Hydrothermal Fluid Flow

In contrast to the three new Pennsylvanian ages for hydrothermal fluid flow, the entire distribution of previously published and new ages from this study reveals that although some hydrothermal fluid flow may coincide with periods of uplift and active orogeny, hydrothermal fluid flow can continue well after the active phase of deformation has ceased. The late Paleozoic to earliest Mesozoic time interval illustrates

this well (fig. 1). The Marathon-Ouachita and Ancestral Rockies deformation began late in the Mississippian and continued until the Early Permian (Wolfcampian; Ye et al., 1996). Some hydrothermal flow events took place during that deformation, but events of hydrothermal fluid flow continued well after the end of the active phase of deformation. The distribution of ages shows dates after the Wolfcampian, continuing through the Permian, and perhaps ending early in the Triassic. These dates coincide with the time before which the Ouachita and Ancestral Rocky Mountains had been fully beveled (Ye et al., 1996). It could indicate that hydrothermal fluid flow was driven by the existence of topographic highs and caused by gravity-driven fluid flow (Garven and Freeze, 1984a, 1984b; Garven, 1993, 1995). By the beginning of the Triassic, the Ouachita mountains had mostly been worn down and, therefore, ceased to provide a hydraulic head that could drive hydrothermal fluids northward. Alternatively, the distribution of ages could be explained by late Permian to early Triassic seismic pumping. Although this is known not to be the timing of most phases of deformation in the region, it is still possible that stresses caused by the Ouachita/Ancestral Rocky Mountains event eventually relaxed and drove fluid flow well after the orogeny.

In considering the tectonic history of the southern midcontinent, one could hypothesize that the initiation of Gulf of Mexico rifting and extension in the Triassic and Jurassic (Salvador, 1991) could have caused domal uplift that could have driven hydrothermal fluid flow, and that extension increased heat flow to the area. In evaluating the distribution of dates, however, there is a dearth of Triassic and Jurassic ages for hydrothermal fluid migration (fig. 1). Thus, the initiation of the Gulf of Mexico apparently did not rejuvenate hydrothermal fluid flow in the midcontinent in a significant way.

Another hypothesis to explain timing of hydrothermal fluid flow (fig. 1) is that the geodynamics that led to Cretaceous intrusives in the midcontinent are drivers for hydrothermal fluid flow in the region. Hypotheses for these intrusives include migration of the North American Plate over the Bermuda Hotspot (Cox and Van Arsdale, 2002), edge-driven convection that led to upwelling of asthenospheric magmas (Kjarsgaard et al., 2017), and the mid-Cretaceous superplume (Larson, 2005). Given the published thermochronology data from Kansas (Blackburn et al., 2008), the geodynamics causing the Cretaceous intrusives there are not likely responsible for hydrothermal fluid migration. Emplacement of these kimberlitic magmas occurred in two pulses during the

Cretaceous. The first pulse emplaced the Tuttle, Stockdale, and Bala kimberlites between 100 and 110 Ma, and the second pulse emplaced the Baldwin Creek kimberlite (and likely the Leonardville kimberlite) at approximately 88±2.7 Ma (Blackburn et al., 2008). Apatite dates from the Tuttle, Stockdale, Bala, and Leonardville kimberlites (67.2±5.1, 67.3±4.4, 64.3±7.5, and 66.1±8, respectively) are much younger than the kimberlite emplacement dates (Blackburn et al., 2008) (table 1). These younger dates cannot be ascribed to heating associated with the intrusives, despite their proximity, and we propose that hydrothermal fluid flow related to the Laramide Orogeny is responsible for reheating the apatites to above closure temperature. Intrusives in Arkansas and other parts of Kansas also date to the Cretaceous, but it is not clear that these intrusives have a regional impact on hydrothermal fluid flow. Fission-track ages of apatites in Paleozoic sedimentary rocks in Arkansas are within the range of the intrusives; however, these dates have been interpreted as a record of uplift and erosion after maximum burial in the Cretaceous (Arne, 1992). Our new age for calcite from the Tri-State Mineral District is Cretaceous (115.6±3.1 Ma); however, it is not proximal to the intrusives.

Our new data from the Tri-State Mineral District (115.6±3.1 Ma) indicate that the known flexure of the midcontinent and/or the distant continental margin uplift of the Sevier orogen affected hydrothermal fluid flow in the midcontinent (question 1 of this study — how does subsurface hydrothermal fluid flow in the midcontinent respond to the tectonic drivers at the continental margins). The distribution of ages of thermal events, compiled from the literature (fig. 1), shows that this process continued during the Laramide Orogeny. Despite the far-field nature of the stress applied by the Sevier and Laramide orogenies to the west of the study area, the Tri-State Mineral District calcite ages indicate that distant deformation at the continental margins and/or flexure in the midcontinent (question 3 — what drives crustal deformation in the midcontinent) can induce hydrothermal fluid flow (question 2 — what drivers have an impact on hydrothermal fluid flow).

Additional drivers for hydrothermal fluid flow are suggested by our model for the Miocene-Pliocene calcite age in the Berexco Wellington KGS 1-32 sample from the Arbuckle Group. This model, as described above, indicates that after uplift in distant areas, a change in climate and the associated increase in the hydraulic head can influence fluid flow across midcontinent strata, particularly if the basement and cover rocks are in hydraulic connection.

Thus, the range of ages (fig. 1) obtained in this study and others suggests that there is no single driver for fluid flow in the midcontinent but that a series of far-field events can affect hydrothermal fluid flow in the midcontinent. Further, we note that high hydraulic head caused by hinterland elevation and climate change can trigger seismicity of critically stressed faults, deformation, and hydrothermal fluid flow in the midcontinent, indicating that a wide range of factors, both tectonic and non-tectonic, can drive hydrothermal fluid flow at various scales in the midcontinent (question 3).

CONCLUSIONS

This paper has demonstrated that the combination of petrography with fluid inclusion studies, strontium isotope geochemistry, and U-Pb LA-ICP-MS dating of carbonate cements is a powerful approach for reconstructing the hidden tectonic and hydrothermal fluid-flow history in cratonal settings. We have presented U-Pb dates from five samples (in three locations) in the midcontinent (figs. 2–3) and compiled and vetted dates for thermally relevant samples to understand what controls hydrothermal fluid migration in Paleozoic strata. We posed three governing questions at the start of this study: (1) How does fluid flow in the midcontinent respond to the tectonic drivers at the continental margins? (2) What drivers have an impact on hydrothermal fluid flow? and (3) What drives crustal deformation in the midcontinent? We conclude the following:

- The midcontinent United States has a complex history of hydrothermal fluid flow due to an array of disparate fluid drivers, deformation, and climate changes.
- A Tri-State Mineral District sample (TSNC 1-14) has an age of 115.6±3.1 Ma, attributed to flexure and distant uplift from the Sevier Orogeny. Based on this and the range of published ages, hydrothermal fluid migration appears to have continued during the Laramide Orogeny (question 1 and 2).
- Calcite cements from Mississippian intervals in the Berexco Wellington KGS 1-32 core (Kansas) and the Blackbird 4-33 core (Oklahoma) yield overlapping dates of 305±10.5 Ma, 305.1±9.1Ma, and 308.6±2.5 Ma. These Late Pennsylvanian ages for hydrothermal fluid flow reveal that some fluid-flow events coincide with the timing of the Marathon-Ouachita Orogeny or Ancestral Rocky Mountains Orogeny. The distribution of published ages shows that some hydrothermal fluid flow continued well after the active phase of deformation, through the Permian

and into the early Triassic. This timing results in two possible explanations: (1) gravity-driven flow from the mountains that lasted until they had been beveled by erosion or (2) relaxation of stress from the orogeny, causing seismic pumping (question 2 and 3).

- A Berexco Wellington KGS 1-32 core sample from the Arbuckle Group has an age of 5.6±1.6 Ma, possibly attributed to fluid flow out of the basement because of increased recharge in an already uplifted hinterland. It is hypothesized that increased fluid pressure in the basement led to seismic pumping from critically stressed faults, leading to discharge of hydrothermal fluids into overlying strata (question 1 and 2).
- Finally, the record of midcontinent hydrothermal fluid flow can be driven either by tectonic (far-field orogenic stress) or non-tectonic drivers, as a function of the geology and hydrology of far-field and surrounding regions. Therefore, there is not a single driver for hydrothermal fluid flow in the midcontinent (question 2).

REFERENCES

Arne, D. C., 1992, Evidence from apatite fission-track analysis for regional Cretaceous cooling in the Ouachita Mountain fold belt and Arkoma Basin of Arkansas: American Association of Petroleum Geologists Bulletin, v. 76, p. 392–402.

Aslan, A., Karlstrom, K. E., Crossey, L. J., Kelley, S., Cole, R., Lazear, G., and Darling, A., 2010, Late Cenozoic evolution of the Colorado Rockies: Evidence for Neogene uplift and drainage integration; in Through the Generations: Geologic and Anthropogenic Field Excursions in the Rocky Mountains from Modern to Ancient, L. A. Morgan and S. L. Quane, eds.: Geological Society of America Field Guide 18, p. 21–54. https://doi.org/10.1130/2010.0018(02)

Bailey, P. A., 2018, Diagenesis of the Arbuckle Group in northeastern and north-central Oklahoma, USA: M.S. thesis, Oklahoma State University, 75 p.

Baksi, A. K., 1997, The timing of Late Cretaceous alkalic igneous activity in the northern Gulf of Mexico basin, southeastern USA: Journal of Geology, v. 105, p. 629–643.

Baldwin, O. D., and Adams, J. A. S., 1971, Potassium-40/argon-40 ages of the alkalic igneous rocks of the Balcones fault trend of Texas: The Texas Journal of Science, v. 22, p. 223–231.

Berendsen, P., and Blair, K. P., 1991, Interpretive subcrop map of the Precambrian basement in the Joplin 1° x 2° quadrangle: Kansas Geological Survey, Subsurface Geology Series 14, 10 p.

Blackburn, T. J., Stockli, D. F., Carlson, R. W., and Berendsen, P., 2008, (U-Th)/He dating of kimberlites — A case study from north-eastern Kansas: Earth and Planetary Science Letters, v. 275, p. 111–120. https://doi.org/10.1016/j.epsl.2008.08.006

Blakey, R. C., and Ranney, W. D., 2018, The continental arc, Sevier Orogeny, Western Interior Seaway and flat-slab subduction: Cretaceous Period: Ca. 145–65 Ma; in Ancient Landscapes of Western North America: A Geologic History with Paleogeographic Maps: Berlin, Springer, p. 103–130. https://doi.org/10.1007/978-3-319-59636-5_8

Blasch, S. R., and Coveney, R. M., Jr., 1988, Goethite bearing brine inclusions, petroleum inclusions, and the geochemical conditions of ore deposition at the Jumbo mine, Kansas: Geochimica et Cosmochimica Acta, v. 52, p. 1,007–1,017.

Brannon, J. C., Cole, S. C., Podosek, F. A., Ragan, V. M., Coveney, R. M., Wallace, M. W., and Bradley, A. J., 1996, Th-Pb and U-Pb dating of ore-stage calcite and Paleozoic fluid flow: Science, v. 271, no. 5,248, p. 491–493.

Brookins, D. G., and Naeser, C. W., 1971, Age of emplacement of Riley County, Kansas, kimberlites and a possible minimum age for the Dakota sandstone: Bulletin of the Geological Society of America, v. 82, p. 1,723–1,726.

Chapin, C. E., 2008, Interplay of oceanographic and paleoclimate events with tectonism during middle to late Miocene sedimentation across the southwestern USA: Geosphere, v. 4, no. 6, p. 976–991. https://doi.org/10.1130/GES00171.1

Coveney, R. M., Ragan, V. M., and Brannon, J. C., 2000, Temporal benchmarks for modeling Phanerozoic flow of basinal brines and hydrocarbons in the southern midcontinent based on radiometrically dated calcite: Geology, v. 28, p. 795–798.

Cox, R. T., and Van Arsdale, R. B., 2002, The Mississippi Embayment, North America: A first order continental structure generated by the Cretaceous superplume mantle event: Journal of Geodynamics, v. 34, p. 163–176. https://doi.org/10.1016/S0264-3707(02)00019-4

DeCelles, P. G., 2004, Late Jurassic to Eocene evolution of the Cordilleran thrust belt and foreland basin system, western USA: American Journal of Science, v. 304, no. 2, p. 105–168.

Dicken, C. L., Pimley, S. G., and Cannon, W. F., 2001, Precambrian basement map of the northern midcontinent, U.S.A. — A digital representation of the 1990 P. K. Sims map: U.S. Geological Survey Open-File Report 01-021, available online only. https://pubs.usgs.gov/of/2001/of01-021/

Duller, R. A., Whittaker, A. C., Swinehart, J. B., Armitage, J. J., Sinclair, H. D., Bair, A., and Allen, P. A., 2012, Abrupt landscape change post–6 Ma on the central Great Plains, USA: Geology, v. 40, no. 10, p. 871–874.

Eaton, G. D., 2008, Epeirogeny in the southern Rocky Mountain region: Evidence and Origin: Geosphere, v. 4, no. 5, p. 764–784.

Eby, G. N., and Vasconcelos, P., 2009, Geochronology of the Arkansas Alkaline Province, Southeastern United States: Journal of Geology, v. 117, p. 615–626. https://doi.org/10.1086/605779

Ellsworth, W. L., 2013, Injection-induced earthquakes: Science, v. 341 (July), p. 1–7.

Flawn, P. T., Goldstein, A., Jr., King, P. B., and Weaver, C. E., 1961, The Ouachita System: Bureau of Economic Geology, The University of Texas, Austin, Texas, p. 401.

Fowler, G. M., 1933, Oil and oil structures in Oklahoma-Kansas zinc-lead mining field: American Association of Petroleum Geology Bulletin 17, p. 1,436–1,445.

Frezon, S. E., and Dixon, G. H., 1975, Texas panhandle and Oklahoma paleotectonic investigations of the Pennsylvanian system in the United States; Part I, Introduction and regional analyses of the Pennsylvanian System: U. S. Geological Survey Professional Paper, p. 177–195.

Garven, G., 1993, Genesis of stratabound ore deposits in the midcontinent basins of North America; 1. The role of regional groundwater flow: The American Journal of Science, v. 293, no. 6, p. 497–568.

Garven, G., 1995, Continental-scale groundwater flow and geologic processes: Annual Review of Earth and Planetary Sciences, v. 23, p. 89–117.

Garven, G., and Freeze, R. A., 1984a, Theoretical analysis of the role of groundwater flow in the genesis of stratabound ore deposits: 1. Mathematical and numerical model: The American Journal of Science, v. 284, no. 10, p. 1,085–1,124.

Garven, G., and Freeze, R. A., 1984b, Theoretical analysis of the role of groundwater flow in the genesis of stratabound ore deposits: 2. Quantitative results: The American Journal of Science, v. 284, no. 10, p. 1,125–1,174.

Garven, G., and Raffensperger, J. P., 1997, Hydrogeology and geochemistry of ore genesis in sedimentary basins; in Geochemistry of Hydrothermal Ore Deposits, 3rd ed., H. L. Barnes (ed.): New York, Wiley, p. 125–189.

Gogineni, S. V., Melton, C. E., and Giardini, A. A., 1978, Some petrological aspects of the Prairie Creek diamond-bearing kimberlite diatreme, Arkansas: Contributions to Mineralogy and Petrology, v. 66, no. 3, p. 251–261. https://doi.org/10.1007/BF00373409

Goldstein, R. H., King, D. B., Watney, W. L., and Pugliano, T. M., 2019, Drivers and history of late fluid flow: Impact on midcontinent reservoir rocks; in Mississippian Reservoirs of the Mid-Continent, U.S.A., G. M. Grammer, J. M. Gregg, J. O. Puckette, P. Jaiswal, M. Pranter, S. J. Mazzullo, and R. H. Goldstein, eds.: American Association of Petroleum Geologists Memoir 122, p. 417–450.

Gregg, J. M., and Shelton, K. L., 2012, Mississippi Valley-type mineralization and ore deposits in the Cambrian–Ordovician great American carbonate bank; in The Great American Carbonate Bank: The Geology and Economic Resources of the Cambrian–Ordovician Sauk Megasequence of Laurentia, J. R. Derby, R. D. Fritz, S. A. Longacre, W. A. Morgan, and C. A. Sternbach, eds.: AAPG Memoir, v. 98, p. 163–186.

Hagni, R. D., 1986, A summary of the geology of the ore deposits of the Tri-State district, Missouri, Kansas, and Oklahoma: A Guidebook to the Geology and Environmental Concerns in the Tri-State Lead-Zinc District, Missouri, Kansas, and Oklahoma: Association of Missouri Geologists, 33rd Annual Meeting and Field Trip, p. 30–54.

Hagni, R. D., and Grawe, O. R., 1964, Mineral paragenesis in the Tri-State district, Missouri, Kansas, Oklahoma: Economic Geology, v. 59, no. 3, p. 449–457.

Hay, R. L., Lee, M., Kolata, D. R., Matthews, J. C., and Morton, J. P., 1988, Episodic potassic diagenesis of Ordovician tuffs in the Mississippi Valley area: Geology, v. 16, p. 743–747.

Heitmann, E. O., Hyland, E. G., Schoettle-Greene, P., Brigham, C. A. P., and Huntington, K. W., 2021, Rise of the Colorado Plateau: A synthesis of paleoelevation constraints from the region and a path forward using temperature-based elevation proxies: Frontiers in Earth Science, v. 9: 648605. https://doi.org/10.3389/feart.2021.648605

Heller, P. L., Bowdler, S. S., Chambers, H. P., Coogan, J. C., Hagen, E. S., Shuster, M. W., Winslow, N. S., and Lawton, T. F., 1986, Time of initial thrusting in the Sevier orogenic belt, Idaho-Wyoming and Utah: *Geology*, v. 14, no. 5, p. 388–391. https://doi.org/10.1130/0091-7613(1986)14<388:TOITIT>2.0.CO;2

Hill, C. A., Polyak, V. J., Asmerom, Y., and Provencio, P., 2016, Constraints on a Late Cretaceous uplift, denudation, and incision of the Grand Canyon region, southwestern Colorado Plateau, USA, from U-Pb dating of lacustrine limestone: Tectonics, v. 35, no. 4, p. 896–906.

Hollenbach, A. M., Mohammadi, S., Goldstein, R. H., and Möller, A., 2021, Hydrothermal fluid flow and burial history in the STACK play of north-central Oklahoma [abstract]; in Midcontinent Carbonate Research Virtual Symposium Extended Abstracts, E. Ortega-Ariza, I. Bode-Omoleye, F. J. Hasiuk, S. Mohammadi, and E. K. Franseen, eds.: Kansas Geological Survey, Technical Series 24, p. 28–30.

Jorgensen, D. G., Helgesen, J. O., and Imes, J. L., 1993, Regional aquifers in Kansas, Nebraska, and parts of Arkansas, Colorado, Missouri, New Mexico, Oklahoma, South Dakota, Texas, and Wyoming — geohydrologic framework: U.S. Geological Survey Professional Paper 1414-B, p.1–72.

Karlstrom, K. E., Coblentz, D., Dueker, K., Ouimet, W., Kirby, E., Van Wijk, J., Schmandt, B., Kelley, S., Lazear, G., Crossey, L. J., Crow, R., Aslan, A., Darling, A., Aster, R., MacCarthy, J., Hansen, S. M., Stachnik, J., Stockli, D. F., Garcia, R. V., Hoffman, M., McKeon, R., Feldman, J., Heizler, M., Donahue, M. S., and the CREST Working Group, 2012, Mantle-driven dynamic uplift of the Rocky Mountains and Colorado Plateau and its surface response: Toward a unified hypothesis: Lithosphere, v. 4, no. 1, p. 3–22; GSA Data Repository Item 2012041. https://doi.org/10.1130/L150.1

Kesler, S. E., Chesley, J. T., Christensen, J. N., Hagni, R. D., Heijlen, W., Kyle, J. R., Muchez, P., Misra, K. C., and van der Voo, R., 2004, Discussion of "Tectonic controls of Mississippi Valley-type lead-zinc mineralization in orogenic forelands" by D. C. Bradley and D. L. Leach: Miner Deposita, v. 39, p. 512–514. https://doi.org/10.1007/s00126-004-0422-3

King, B., 2013, Fluid flow, thermal history, and diagenesis of the Cambrian-Ordovician Arbuckle Group and overlying units in south-central Kansas: M.S. thesis, University of Kansas, Lawrence, Kansas, 288 p.

King, B. D., and Goldstein, R. H., 2018, History of hydrothermal fluid flow in the midcontinent, USA: The relationship between inverted thermal structure, unconformities and porosity distribution; in Reservoir Quality of Clastic and Carbonate Rocks: Analysis, Modelling and Prediction, P. J. Armitage, A. R. Butcher, J. M. Churchill, A. E. Csoma, C. Hollis, R. H. Lander, J. E. Omma, and R. H. Worden, eds.: Geological Society, London, Special Publications, 435, first published online in 2016, p. 283–329.

Kjarsgaard, B. A., Heaman, L. M., Sarkar, C., and Pearson, D. G., 2017, The North American mid-Cretaceous kimberlite corridor: Wet, edge-driven decompression melting of an OIB-type deep mantle source: Geochemistry, Geophysics, Geosystems, v. 18, p. 2,727–2,747. https://doi.org/10.1002/2016GC006761

Kluth, C. F., and Coney, P. J., 1981, Plate tectonics of the Ancestral Rocky Mountains: Geology, v. 9, p. 10–15.

Larson, R. L., 2005, The Mid-Cretaceous superplume episode: Scientific American, v. 272, no. 2, p. 82–86. https://doi.org/10.1038/scientificamerican0705-22sp

Leach, D. L., Bradley, D., Lewchuk, M. T., Symons, D. T. A., de Marsily, G., and Brannon, J., 2001, Mississippi Valley-type lead-zinc deposits through geological time: Implications from recent age-dating research: Minerlium Deposita, v. 36, p. 711–740.

Leach, D. L., Taylor, R. D., Fey, D. L., Diehl, S. F., and Saltus, R. W., 2010, A deposit model for Mississippi Valley-type lead-zinc ores: Scientific Investigations Report 5070-A, U.S. Geological Survey, Reston, Virginia, 64 p.

Lukens, W. E., Fox, D. L., Snell, K. E., Wiest, L. A., Layzell, A. L., Uno, K. T., Polissar, P. J., Martin, R. A., Fox-Dobbs, K., and Ez-Campomanes, P. P., 2019, Pliocene paleoenvironments in the Meade basin, southwest Kansas, U.S.A.: Journal of Sedimentary Research, v. 89, p. 416–439. http://dx.doi.org/10.2110/jsr.2019.24

Marshak, S., Nelson, W. J., and McBride, J. H., 2003, Phanerozoic strike-slip faulting in the continental interior platform of the United States: Examples from the Laramide Orogen, Midcontinent, and Ancestral Rocky Mountains: Geological Society, London, Special Publications, v. 210, no. 1, p. 159–184.

McMillan, M. E., Angevine, C. L., and Heller, P. L., 2002, Post-depositional tilt of the Miocene-Pliocene Ogallala Group on the western Great Plains: Evidence of late Cenozoic uplift of the Rocky Mountains: Geology, v. 30, p. 63–66. https://doi.org/10.1130/0091-7613(2002)030<0063:PTOTMP>2.0.CO;2

Mohammadi, S., Ewald, T. A., Gregg, J. M., and Shelton, K. L., 2019a, Diagenesis of Mississippian carbonate rocks in north-central Oklahoma, USA; in Mississippian Reservoirs of the Mid-Continent, U.S.A., G. M. Grammer, J. M. Gregg, J. O. Puckette, P. Jaiswal, M. Pranter, S. J. Mazzullo, and R. H. Goldstein, eds.: American Association of Petroleum Geologists Memoir 122, p. 353–358.

Mohammadi, S., Gregg, J. M., Shelton, K. L., Appold, M. S., and Puckette, J. O., 2019b, Influence of late diagenetic fluids on Mississippian carbonate rocks on the Cherokee–Ozark Platform, NE Oklahoma, NW Arkansas, SW Missouri, and SE Kansas; in Mississippian Reservoirs of the Mid-Continent, U.S.A., G. M. Grammer, J. M. Gregg, J. O. Puckette, P. Jaiswal, M. Pranter, S. J. Mazzullo, and R. H. Goldstein, eds.: American Association of Petroleum Geologists Memoir 122, p. 323–352.

Musgrove, M. L., and Banner, J. L., 1993, Regional ground-water mixing and origin of saline fluids: Midcontinent, United States: Science, v. 259, p. 1,877–1,882.

Noble, E. A., 1963, Formation of ore deposits by water of compaction: Economic Geology, v. 58, p. 1,145–1,156.

Northcutt, R. A., and Campbell, J. A., 1996, Geologic provinces of Oklahoma: The Shale Shaker, v. 46, p. 99–103.

Pan, H., and Symons, D. T. A., 1990, Paleomagnetism of the Mississippi Valley-type ores and host rocks in the northern Arkansas and Tri-State districts: Canadian Journal of Earth Science, v. 27, p. 923–931.

Paradis, S., Hannigan, P., and Dewing, K., 2008, Mississippi Valley-type lead-zinc deposits (MVT), Ottawa: Geological Survey of Canada, p. 1–15.

Paton, C., Hellstrom, J., Paul, B., Woodhead, J., and Hergt, J., 2011, Iolite: Freeware for the visualisation and processing of mass spectrometry data: Journal of Analytical Atomic Spectrometry, v. 26, p. 2,508–2,518.

Paton, C., Woodhead, J. D., Hellstrom, J. C., Hergt, J. M., Greig, A., and Maas, R., 2010, Improved laser ablation U-Pb zircon geochronology through robust downhole fractionation correction: Geochemistry, Geophysics, Geosystems, v. 11, no. 3. https://doi.org/10.1029/2009GC002618

Ramaker, E. M., Goldstein, R. H., Franseen, E. K., and Watney, W. L., 2015, What controls porosity in cherty fine-grained carbonate reservoir rocks? Impact of stratigraphy, unconformities, structural setting and hydrothermal fluid flow: Mississippian, SE Kansas: The Geological Society of London, Special Publications, v. 406, p. 179–208.

Ridge, J., 1936, The genesis of the Tri-State zinc and lead ores: Economic Geology, v. 31, no. 3, p. 298–313. https://doi.org/10.2113/gsecongeo.31.3.298

Roberts, N. M. W., Rasbury, T. E., Parrish, R. R., Smith, C. J., Horstwood, M. S. A., and Condon, D.J., 2017, A calcite reference material for LA-ICP-MS U-Pb geochronology: Geochemistry, Geophysics, Geosystems, v. 18, p. 2,807–2,814.

Rothbard, D. R., 1983, Diagenetic history of the Lamotte Sandstone, Southeast Missouri; in International Conference on Mississippi Valley Type Lead-Zinc Deposits: Rolla, Mo., University of Missouri-Rolla, p. 385–395.

Sahagian, D., Proussevitch, A., and Carlson, W., 2002, Timing of Colorado Plateau uplift: Initial constraints from vesicular basalt-derived paleoelevations: Geology, v. 30, no. 9, p. 807–810.

Salvador, A., 1991, Origin and development of the Gulf of Mexico basin; in The Gulf of Mexico Basin, A. Salvador, ed.: Geological Society of America, p. 389–444.

Scharon, L., and Hsu, I., 1969, Paleomagnetic investigation of some Arkansas alkalic igneous rocks: Journal of Geophysical Research, v. 74, p. 2,774–2,779.

Schmidt, R. A., 1962, Temperatures of mineral formation in the Miami-Picher District as indicated by liquid inclusions: Economic Geology, v. 57, p. 1–20.

Schoenball, M., Walsh, F. R., Weingarten, M., and Ellsworth, W. L., 2018, How faults wake up: The Guthrie-Langston, Oklahoma earthquakes: Leading Edge, v. 37, p. 100–106. https://doi.org/10.1190/tle37020100.1

Shelton, K. L., Bauer, R. M., and Gregg, J. M., 1992, Fluid-inclusion studies of regionally extensive epigenetic dolomites, Bonneterre Dolomite (Cambrian), southeast Missouri: Evidence of multiple fluids during dolomitization and lead-zinc mineralization: Geological Society of America Bulletin, v. 104, p. 675–683.

Shelton, K. L., Reader, J. M., Ross, L. M., Viele, G. W., and Seidemann, D. E., 1986, Ba-rich adularia from the Ouachita Mountains, Arkansas: Implications for a post-collisional hydrothermal system: American Mineralogist, v. 71, p. 916–923.

Sibson, R. H., Moore, J. M., and Rankin, A. H., 1975, Seismic pumping — A hydrothermal fluid transport mechanism: Journal of the Geological Society, v. 131, p. 653–659.

Symons, D. T. A., Lewchuk, M. T., and Leach, D. L., 1998, Age and duration of the Mississippi Valley-type mineralizing fluid flow event in the Viburnum Trend, southeast Missouri, USA, determined from palaeomagnetism: Geological Society, London, Special Publications, v. 144, p. 27–39.

Symons, D. T. A., and Sangster, D. F., 1991, Paleomagnetic age of the central Missouri barite deposits and its genetic implications: Economic Geology, v. 86, p. 1–12.

Taylor, W. J., Bartley, J. M., Martin, M. W., Geissman, J. W., Walker, J. D., Armstrong, P. A., and Fryxell, J. E., 2000, Relations between hinterland and foreland shortening: Sevier Orogeny, central North American Cordillera: Tectonics, v. 19, no. 6, p. 1,124–1,143.

Temple, B. J., Bailey, P. A., and Gregg, J. M., 2020, Carbonate diagenesis of the Arbuckle Group north central Oklahoma to southeastern Missouri: The Shale Shaker, v. 71, no. 1, 30 p.

Tennyson, R., Brahana, V., Polyak, V. J., Potra, A., Covington, M., Asmerom, Y., Terry, J., Pollock, E., and Decker, D. D., 2017, Hypogene speleogenesis in the southern Ozark uplands, mid-continental United States; in Hypogene Karst Regions and Caves of the World, Cave and Karst Systems of the World, A. N. Klimchouk, A. Palmer, J. S. De Waele, A. Auler, and P. Audra, eds.: Berlin, Springer International, p. 663–676.

Townend, J., and Zoback, M. D., 2000, How faulting keeps the crust strong: Geology, v. 28, no. 5, p. 399–402.

USGS, 2020, GMNA Resources: Geologic Map of North America GIS database. https://ngmdb.usgs.gov/gmna/#gmnaDocs

Walton, A. W., Wojcik, K. M., Goldstein, R. H., and Barker, C. E., 1995, Diagenesis of Upper Carboniferous rocks in the Ouachita foreland shelf in the mid-continent USA: An overview of widespread effects of a Variscan-equivalent orogeny: Geologische Rundschau, v. 84, p. 535–551.

Wells, M. L., Hoisch, T. D., Cruz-Uribe, A. M., and Vervoort, J. D., 2012, Geodynamics of synconvergent extension and tectonic mode switching: Constraints from the Sevier-

Laramide orogen: Tectonics, v. 31, no. 1, p. 1–20. https://doi.org/10.1029/2011TC002913

Wenz, Z. J., Appold, M. S., Shelton, K. L., and Tesfaye, S., 2012, Geochemistry of Mississippi Valley-type mineralizing fluids of the Ozark Plateau: A regional synthesis: American Journal of Science, v. 312, p. 22–80.

Wheeler, J. R., 1989, K-Ar dating of authigenic K-Feldspar in the Butterly Dolomite (Lower Ordovician), Arbuckle Uplift: Evidence of Late Pennslvanian-Early Permian tectonically-induced diagenesis and implications for timing of Mississippi Valley-type mineralization: M. S. thesis, University of Tulsa, 135 p.

Wisniowiecki, M. J., Van der Voo, R., McCabe, C., and Kelly, W. C., 1983, A Pennsylvanian paleomagnetic pole from the mineralized Late Cambrian Bonneterre Formation, southeast Missouri: Journal of Geophysical Research, Solid Earth, v. 88, no. B8, p. 6,540–6,548.

Woodhead, J. D., and Hergt, J. M., 2001, Strontium, neodymium and lead isotope analyses of NIST glass certified reference materials: SRM 610, 612, 614: Geostandards Newsletter, v. 25, no. 2-3, p. 261–266.

Ye, H., Royden, L., Burchfiel, C., and Schuepbach, M., 1996, Late Paleozoic deformation of interior North America: The Greater Ancestral Rocky Mountains: AAPG Bulletin, v. 80, no. 9, p. 1,397–1,432.

Yonkee, W. A., and Weil, A. B., 2015, Tectonic evolution of the Sevier and Laramide belts within the North American Cordillera orogenic system: Earth-Science Reviews, v. 150, p. 531–593.

Zartman, R. E., 1977, Geochronology of some alkalic rock provinces in eastern and central United States: Annual Review of Earth and Planetary Science, v. 5, p. 257–286. https://doi.org/10.1146/annurev.ea.05.050177.001353

Zartman, R. E., Brock, M. R., Heyl, A. V., and Thomas, H. H., 1967, K-Ar and Rb-Sr ages of some alkalic intrusive rocks from central and eastern United States: American Journal of Science, v. 265, no. 10, p. 848–870.

Zartman, R. E., and Howard, J. M., 1987, Uranium-lead age of large zircon crystals from the Potash Sulfur Springs igneous complex, Garland County, Arkansas; in Mantle Metasomatism and Alkaline Magmatism, E. M. Morris and J. D. Pasteris, eds.: Geological Society of America Special Paper 215, p. 235–240.

Table S1: Supplementary table U-Pb data

Samples from Wellington KGS 1-32 core (5,061.5 ft)

	$^{238}U/^{206}Pb$ correct.*	Prop2SE	$^{207}Pb/^{206}Pb$ correct.*	Prop2SE	err. corr. rho	U ppm	±	Th ppm	±	Pb ppm	±
1	665.02	94.37	0.320	0.120	0.819	0.205	0.007	0.167	0.004	0.0007	0.0002
2	23.05	3.82	0.860	0.130	0.313	0.071	0.002	0.031	0.002	0.0114	0.0023
3	12.69	2.51	0.795	0.069	0.245	0.119	0.002	0.023	0.001	0.0335	0.0078
4	2.91	0.21	0.768	0.021	0.486	0.086	0.006	0.024	0.002	0.1016	0.0096
5	574.97	279.06	0.440	0.370	0.46	0.057	0.001	0.045	0.002	0.0006	0.0005
6	262.84	87.98	0.690	0.610	0.285	0.030	0.001	0.012	0.001	0.0002	0.0002
7	204.43	64.66	0.500	0.170	0.327	0.117	0.002	0.075	0.004	0.0010	0.0003
8	375.49	99.01	0.400	0.250	0.668	0.114	0.002	0.099	0.004	0.0005	0.0004
9	438.07	81.09	0.730	0.360	-0.005	0.239	0.004	0.183	0.004	0.0011	0.0007
10	530.74	186.98	0.300	0.220	-0.107	0.158	0.003	0.130	0.004	0.0002	0.0004
11	484.18	107.21	0.570	0.490	0.095	0.131	0.002	0.094	0.002	0.0004	0.0003
12	50.18	25.14	0.770	0.210	0.353	0.155	0.002	0.337	0.008	0.0051	0.0010
13	19.85	2.06	0.843	0.097	0.062	0.124	0.004	0.329	0.007	0.0213	0.0026
14	0.67	0.07	0.787	0.018	0.432	0.072	0.003	0.022	0.002	0.3770	0.0350
15	959.95	335.19	0.370	0.260	0.691	0.095	0.001	0.032	0.001	0.0003	0.0002
16	0.69	0.14	0.730	0.029	0.075	0.062	0.003	0.038	0.003	0.2930	0.0760

* isotope ratios corrected by calibration of Pb isotope ratio to NIST 614 glass, U-Pb ratio to WC1 carbonate reference material (Roberts et al., 2017).

Note: Some results, not shown above, were omitted from calculation of the discordia line based on the following criteria:

1. Uncertainty on $^{207}Pb/^{206}Pb$ is equal to or higher than the ratio
2. $^{207}Pb/^{206}Pb$ is a geologically impossible value
3. High uncertainty
4. Influential point leveraging discordia line
5. Petrographic observation of laser spot position indicates open system or mixing (e.g., inclusion, grain boundary, recrystallized area)

Sample from Tri-State Mineral District (TSNC 1-14)

	$^{238}U/^{206}Pb$ correct.*	Prop2SE	$^{207}Pb/^{206}Pb$ correct.*	Prop2SE	U ppm	±	Th ppm	±	Pb ppm	±
1	48.84	6.21	0.058	0.012	0.277	0.014	0.026	0.0011	0.0023	0.0037
2	53.81	3.77	0.071	0.026	0.114	0.004	0.024	0.0013	0.0005	0.0003
3	51.14	3.03	0.083	0.014	0.201	0.004	0.003	0.0003	0.0008	0.0003
4	52.48	3.59	0.092	0.031	0.112	0.008	0.039	0.0036	0.0008	0.0003
5	48.56	3.35	0.100	0.027	0.088	0.005	0.011	0.0007	0.0005	0.0002
6	52.48	3.91	0.106	0.033	0.073	0.003	0.050	0.0015	0.0010	0.0004
7	51.30	2.87	0.106	0.017	0.137	0.003	0.001	0.0002	0.0003	0.0002
8	46.17	7.57	0.109	0.058	0.033	0.001	0.012	0.0007	0.0002	0.0002
9	45.67	6.42	0.116	0.057	0.028	0.001	0.014	0.0006	0.0003	0.0002
10	40.62	6.05	0.122	0.066	0.021	0.001	0.023	0.0010	0.0004	0.0003
11	46.94	7.3	0.164	0.100	0.035	0.001	0.001	0.0002	0.0002	0.0003
12	42.03	7.53	0.168	0.017	0.295	0.028	0.006	0.0004	0.0037	0.0005
13	41.21	5.63	0.171	0.048	0.044	0.002	0.026	0.0012	0.0008	0.0003
14	47.47	5.33	0.177	0.098	0.067	0.003	0.039	0.0023	0.0009	0.0003
15	52.48	9.45	0.178	0.092	0.027	0.001	0.023	0.0010	0.0007	0.0003
16	42.67	9.27	0.180	0.120	0.026	0.002	0.002	0.0003	0.0002	0.0002
17	37.06	6.34	0.220	0.130	0.021	0.003	0.032	0.0017	0.0006	0.0003
18	38.40	3.67	0.256	0.063	0.061	0.002	0.026	0.0023	0.0016	0.0003
19	30.72	6.48	0.276	0.037	0.155	0.024	0.003	0.0003	0.0051	0.0010
20	31.06	4.11	0.284	0.063	0.064	0.002	0.034	0.0009	0.0035	0.0011
21	31.53	2.94	0.324	0.052	0.049	0.004	0.036	0.0034	0.0030	0.0006
22	29.65	2.7	0.387	0.070	0.052	0.004	0.028	0.0025	0.0032	0.0005
23	9.68	0.49	0.528	0.023	0.062	0.004	0.032	0.0019	0.0163	0.0013
24	12.86	1.29	0.528	0.065	0.027	0.002	0.014	0.0011	0.0054	0.0007
25	3.79	1	0.602	0.056	0.019	0.001	0.002	0.0006	0.0163	0.0048
26	3.42	0.71	0.649	0.050	0.038	0.001	0.011	0.0007	0.0336	0.0073

* isotope ratios corrected by calibration of Pb isotope ratio to NIST 614 glass, U-Pb ratio to WC1 carbonate reference material (Roberts et al., 2017).

Note: Some results, not shown above, were omitted from calculation of the discordia line based on the following criteria:
1. Uncertainty on $^{207}Pb/^{206}Pb$ is equal to or higher than the ratio
2. $^{207}Pb/^{206}Pb$ is a geologically impossible value
3. High uncertainty
4. Influential point leveraging discordia line
5. Petrographic observation of laser spot position indicates open system or mixing (e.g., inclusion, grain boundary, recrystallized area)

Sample from Wellington KGS 1-32 core (3775.5 ft)

	^{238}U/^{206}Pb correct.*	Prop2SE	^{207}Pb/^{206}Pb correct.*	Prop2SE	err. corr. rho	U ppm	±	Th ppm	±	Pb ppm	±
1	16.65	1.24	0.162	0.030	-0.19	0.0764	0.0026	0.0035	0.0004	0.0021	0.0005
2	20.14	1.23	0.098	0.026	0.094	0.0445	0.0006	0.0004	0.0001	0.0002	0.0002
3	17.95	1.08	0.153	0.038	0.15	0.0339	0.0006	0.0003	0.0001	0.0005	0.0003
4	16.19	1.92	0.289	0.065	0.36	0.0119	0.0011	bdl	-	0.0009	0.0003
5	12.99	1.58	0.500	0.200	0.153	0.0121	0.0011	bdl	-	0.0022	0.0006
6	6.69	1.27	0.600	0.110	-0.062	0.0089	0.0005	bdl	-	0.0034	0.0007
7	6.46	0.60	0.615	0.092	-0.01	0.0074	0.0006	bdl	-	0.0038	0.0007
8	3.35	1.93	0.880	0.670	0.006	0.0006	0.0001	bdl	-	0.0003	0.0002
9	2.25	0.97	0.580	0.280	0.854	0.0004	0.0001	bdl	-	0.0005	0.0004
10	1.35	0.77	0.870	0.560	0.773	0.0001	0.0000	bdl	-	0.0005	0.0002
11	16.23	2.44	0.380	0.120	0.298	0.0052	0.0005	bdl	-	0.0003	0.0002
12	14.96	1.96	0.300	0.140	0.809	0.0069	0.0004	bdl	-	0.0003	0.0002
13	13.80	3.13	0.400	0.300	0.124	0.0093	0.0005	0.0001	0.0001	0.0004	0.0004
14	16.73	3.33	0.165	0.078	0.531	0.0082	0.0005	bdl	-	0.0002	0.0003
15	21.11	4.05	0.096	0.077	0.183	0.0074	0.0003	0.0006	0.0002	0.0000	0.0002
16	7.26	1.92	0.460	0.180	0.108	0.0030	0.0003	bdl	-	0.0007	0.0005
17	14.70	1.04	0.271	0.031	0.204	0.0324	0.0006	0.0002	0.0001	0.0025	0.0004
18	18.19	1.71	0.259	0.042	-0.152	0.0172	0.0004	0.0005	0.0002	0.0008	0.0003
19	17.22	1.15	0.117	0.015	0.309	0.0383	0.0007	0.0015	0.0002	0.0013	0.0003
20	13.14	1.11	0.404	0.054	0.016	0.0226	0.0009	0.0026	0.0003	0.0023	0.0004
21	0.55	0.17	0.750	0.240	0.451	0.0002	0.0000	bdl	-	0.0019	0.0004
22	15.66	1.65	0.329	0.085	0.443	0.0140	0.0005	0.0014	0.0003	0.0007	0.0004
23	10.22	1.27	0.640	0.370	0.162	0.0050	0.0002	bdl	-	0.0010	0.0003
24	12.39	1.28	0.366	0.050	0.558	0.0125	0.0005	0.0005	0.0002	0.0016	0.0004
25	16.80	1.57	0.260	0.140	0.112	0.0123	0.0003	0.0001	0.0001	0.0008	0.0003
26	0.96	0.37	0.880	0.210	0.522	0.0009	0.0001	bdl	-	0.0024	0.0004
27	16.73	3.59	0.220	0.160	0.325	0.0090	0.0006	bdl	-	0.0002	0.0003
28	14.96	1.38	0.239	0.040	0.238	0.0138	0.0004	0.0009	0.0002	0.0006	0.0003
29	17.17	1.22	0.176	0.028	0.459	0.0311	0.0012	0.0032	0.0004	0.0008	0.0002
30	15.21	0.87	0.309	0.047	0.156	0.0608	0.0020	0.0022	0.0004	0.0045	0.0007

* isotope ratios corrected by calibration of Pb isotope ratio to NIST 614 glass, U-Pb ratio to WC1 carbonate reference material (Roberts et al., 2017).

Note: Some results, not shown above, were omitted from calculation of the discordia line based on the following criteria:
1. Uncertainty on ^{207}Pb/^{206}Pb is equal to or higher than the ratio
2. ^{207}Pb/^{206}Pb is a geologically impossible value
3. High uncertainty
4. Influential point leveraging discordia line
5. Petrographic observation of laser spot position indicates open system or mixing (e.g., inclusion, grain boundary, recrystallized area)

bdl: below detection limit

Sample from Wellington KGS 1-32 core (3758.9 ft)

	^{238}U/^{206}Pb correct.*	Prop2SE	^{207}Pb/^{206}Pb correct.*	Prop2SE	err. corr. rho	U ppm	±	Th ppm	±	Pb ppm	±
1	0.18	0.01	0.860	0.015	0.533	0.1600	0.0260	0.3010	0.0260	3.6900	0.5900
2	0.52	0.06	0.823	0.041	0.627	0.0110	0.0005	0.0008	0.0003	0.0702	0.0054
3	0.18	0.01	0.847	0.020	-0.128	0.0810	0.0260	0.1390	0.0430	1.7800	0.5900
4	0.23	0.02	0.801	0.029	0.526	0.0070	0.0013	0.0032	0.0009	0.1150	0.0340
5	0.94	0.09	0.792	0.058	0.142	0.0040	0.0003	0.0003	0.0001	0.0146	0.0013
6	1.49	0.18	0.796	0.078	0.231	0.0052	0.0004	0.0005	0.0003	0.0122	0.0015
7	14.88	1.38	0.303	0.057	0.197	0.0152	0.0004	0.0019	0.0003	0.0013	0.0004
8	1.36	0.27	0.830	0.140	-0.029	0.0013	0.0001	bdl	-	0.0028	0.0004
9	9.33	0.62	0.435	0.044	0.399	0.0231	0.0008	0.0003	0.0001	0.0058	0.0010
10	12.39	1.36	0.440	0.150	-0.063	0.0216	0.0007	0.0007	0.0003	0.0027	0.0008
11	11.92	0.83	0.414	0.051	-0.064	0.0204	0.0006	0.0010	0.0004	0.0037	0.0008
12	7.22	0.74	0.545	0.054	0.704	0.0165	0.0004	0.0009	0.0002	0.0057	0.0007
13	2.46	0.49	0.762	0.080	0.406	0.0044	0.0004	0.0002	0.0001	0.0170	0.0230
14	8.72	0.70	0.580	0.073	0.005	0.0120	0.0005	0.0004	0.0001	0.0032	0.0004
15	10.37	0.76	0.509	0.090	0.436	0.0139	0.0004	0.0004	0.0001	0.0029	0.0005
16	8.06	0.69	0.553	0.070	0.066	0.0120	0.0003	0.0001	0.0001	0.0032	0.0005
17	10.13	1.16	0.510	0.140	0.419	0.0289	0.0007	0.0003	0.0001	0.0050	0.0011
18	10.88	0.82	0.393	0.061	-0.207	0.0210	0.0006	0.0003	0.0002	0.0042	0.0007
19	0.18	0.03	0.812	0.019	0.301	0.1750	0.0150	0.1373	0.0080	3.3700	0.2900
20	2.12	0.23	0.752	0.017	0.045	0.1830	0.0170	0.1590	0.0180	0.3000	0.0400
21	14.23	1.24	0.286	0.044	0.210	0.0281	0.0009	0.0004	0.0002	0.0021	0.0005
22	11.16	1.09	0.520	0.150	0.028	0.0225	0.0012	0.0005	0.0002	0.0035	0.0005
23	14.76	1.25	0.287	0.049	0.334	0.0297	0.0012	0.0009	0.0004	0.0026	0.0008
24	0.20	0.02	0.812	0.010	0.044	0.0689	0.0072	0.0229	0.0047	1.3800	0.1800
25	13.66	1.11	0.262	0.040	0.425	0.0200	0.0005	0.0012	0.0003	0.0019	0.0005
26	14.30	0.81	0.259	0.020	0.132	0.0850	0.0026	0.0039	0.0006	0.0066	0.0011
27	12.42	1.09	0.430	0.110	0.164	0.0605	0.0030	0.0024	0.0007	0.0077	0.0011
28	13.87	1.52	0.375	0.067	0.317	0.0141	0.0007	0.0026	0.0005	0.0014	0.0007
29	13.83	0.74	0.277	0.033	0.016	0.0398	0.0011	0.0052	0.0005	0.0031	0.0005
30	16.68	1.04	0.178	0.024	-0.021	0.0980	0.0021	0.0077	0.0009	0.0044	0.0009
31	18.97	1.03	0.105	0.014	0.261	0.1153	0.0020	0.0092	0.0007	0.0031	0.0009
32	13.03	1.12	0.315	0.039	-0.008	0.0296	0.0011	0.0009	0.0002	0.0030	0.0004
33	16.93	1.02	0.260	0.110	0.084	0.0656	0.0013	0.0052	0.0006	0.0022	0.0006
34	18.87	1.56	0.156	0.025	-0.391	0.0597	0.0020	0.0037	0.0008	0.0010	0.0006
35	15.44	0.89	0.248	0.086	-0.044	0.0437	0.0007	0.0043	0.0004	0.0022	0.0004
36	12.75	1.10	0.360	0.200	0.087	0.0368	0.0008	0.0017	0.0003	0.0028	0.0008
37	10.06	0.66	0.471	0.060	-0.079	0.0390	0.0012	0.0035	0.0004	0.0065	0.0007
38	16.70	0.98	0.221	0.085	0.012	0.0455	0.0009	0.0049	0.0006	0.0021	0.0004

39	17.47	1.25	0.222	0.047	-0.053	0.0721	0.0012	0.0035	0.0004	0.0022	0.0004
40	15.64	1.21	0.352	0.099	0.180	0.0238	0.0008	0.0013	0.0002	0.0016	0.0004
41	17.06	1.25	0.144	0.020	0.299	0.0386	0.0022	0.0019	0.0003	0.0014	0.0004
42	1.62	0.15	0.759	0.052	0.354	0.0131	0.0027	0.0024	0.0006	0.0283	0.0060
43	1.52	0.16	0.838	0.088	0.346	0.0045	0.0003	0.0012	0.0002	0.0095	0.0017
44	1.30	0.17	0.776	0.086	0.263	0.0024	0.0002	0.0001	0.0001	0.0061	0.0010
45	6.13	0.48	0.670	0.140	-0.027	0.0116	0.0003	0.0010	0.0002	0.0047	0.0005
46	11.61	1.09	0.392	0.042	-0.001	0.0238	0.0006	0.0007	0.0002	0.0036	0.0006
47	8.18	1.00	0.531	0.058	0.220	0.0523	0.0009	0.0019	0.0005	0.0130	0.0025
48	12.43	1.09	0.390	0.055	0.619	0.0438	0.0010	0.0020	0.0007	0.0068	0.0011

* isotope ratios corrected by calibration of Pb isotope ratio to NIST 614 glass, U-Pb ratio to WC1 carbonate reference material (Roberts et al., 2017).

Note: Some results, not shown above, were omitted from calculation of the discordia line based on the following criteria:
1. Uncertainty on $^{207}Pb/^{206}Pb$ is equal to or higher than the ratio
2. $^{207}Pb/^{206}Pb$ is a geologically impossible value
3. High uncertainty
4. Influential point leveraging discordia line
5. Petrographic observation of laser spot position indicates open system or mixing (e.g., inclusion, grain boundary, recrystallized area)

bdl: below detection limit

Sample: Blackbird 4-33 core (3370.9 ft)

	^{238}U/^{206}Pb correct.*	Prop2SE	^{207}Pb/^{206}Pb correct.*	Prop2SE	U ppm	±	Th ppm	±	Pb ppm	±
1	19.76	0.42	0.066	0.006	0.4605	0.0070	0.0089	0.0005	0.0020	0.0006
2	19.93	0.41	0.069	0.004	1.1060	0.0160	0.0124	0.0005	0.0053	0.0012
3	20.51	1.29	0.072	0.020	0.0466	0.0025	0.0006	0.0002	0.0003	0.0003
4	19.94	0.37	0.073	0.005	0.7820	0.0280	0.0085	0.0005	0.0042	0.0006
5	20.02	0.76	0.073	0.011	0.3720	0.0100	0.0145	0.0011	0.0017	0.0006
6	19.77	0.34	0.077	0.005	0.4880	0.0150	0.0033	0.0003	0.0036	0.0008
7	19.25	1.45	0.084	0.023	0.0443	0.0025	0.0005	0.0001	0.0007	0.0004
8	19.88	0.80	0.085	0.012	0.1715	0.0028	0.0049	0.0004	0.0016	0.0007
9	19.38	0.71	0.087	0.011	0.3290	0.0150	0.0071	0.0005	0.0033	0.0010
10	18.90	0.47	0.094	0.008	0.4140	0.0076	0.0091	0.0006	0.0050	0.0009
11	19.07	1.08	0.097	0.013	0.1983	0.0097	0.0029	0.0003	0.0028	0.0008
12	18.82	1.09	0.098	0.021	0.0636	0.0016	0.0012	0.0002	0.0013	0.0004
13	19.97	1.46	0.102	0.026	0.0410	0.0018	0.0010	0.0002	0.0007	0.0004
14	18.65	0.99	0.123	0.023	0.0546	0.0015	0.0031	0.0003	0.0009	0.0003
15	17.28	0.74	0.140	0.019	0.1313	0.0032	0.0024	0.0003	0.0044	0.0010
16	17.17	0.73	0.150	0.018	0.3408	0.0092	0.0114	0.0009	0.0112	0.0013
17	16.93	0.85	0.229	0.025	0.0864	0.0019	0.0032	0.0004	0.0039	0.0006
18	14.72	1.05	0.239	0.026	0.0669	0.0015	0.0032	0.0003	0.0043	0.0006
19	13.99	1.76	0.297	0.063	0.0140	0.0004	0.0005	0.0001	0.0015	0.0004
20	13.45	1.18	0.322	0.041	0.0171	0.0007	bdl	-	0.0014	0.0004
21	9.10	0.48	0.455	0.035	0.0366	0.0012	0.0006	0.0001	0.0081	0.0010
22	6.55	3.00	0.486	0.091	0.0142	0.0006	0.0003	0.0001	0.0032	0.0007
23	6.26	1.76	0.550	0.100	0.0317	0.0015	0.0017	0.0030	0.0151	0.0063
24	4.64	0.38	0.588	0.036	0.0500	0.0015	0.0018	0.0002	0.0303	0.0037
25	5.95	0.71	0.594	0.065	0.0239	0.0012	0.0005	0.0001	0.0103	0.0014
26	3.38	0.36	0.680	0.041	0.0149	0.0005	0.0002	0.0001	0.0148	0.0021

* isotope ratios corrected by calibration of Pb isotope ratio to NIST 614 glass, U-Pb ratio to WC1 carbonate reference material (Roberts et al., 2017).

Note: Some results, not shown above, were omitted from calculation of the discordia line based on the following criteria:
1. Uncertainty on ^{207}Pb/^{206}Pb is equal to or higher than the ratio
2. ^{207}Pb/^{206}Pb is a geologically impossible value
3. High uncertainty
4. Influential point leveraging discordia line
5. Petrographic observation of laser spot position indicates open system or mixing (e.g., inclusion, grain boundary, recrystallized area)

bdl: below detection limit

Midcontinent Geoscience • Volume 3 • August 2022
Tony Layzell — Editor

Guest Editor — Ibukun Bode-Omoleye
Technical Editor — Julie Tollefson

Midcontinent Geoscience is an open-access, peer-reviewed journal of the Kansas Geological Survey. The journal publishes original research on a broad array of geoscience topics, with an emphasis on the midcontinent region of the United States, including the Great Plains and Central Lowland provinces.

Submission information: https://journals.ku.edu/mg/about/submissions

KANSAS GEOLOGICAL SURVEY

The University of Kansas